Comparison of the H_2O, HDO and δD stratospheric climatologies between the MIPAS-ESA v8, MIPAS-IMK v5 and ACE-FTS Vv4.1/4.2 satellite data sets

Karen De Los Ríos[1,2], Paulina Ordoñez[3,2], Gabriele P. Stiller[4], Piera Raspollini[5], Marco Gai[5], Kaley A. Walker[6], Cristina Peña-Ortiz[3], and Luis Acosta[1,7]

[1]Instituto de Física, Universidad Nacional Autónoma de México, Mexico City, 04510, Mexico
[2]Instituto de Ciencias de la Atmósfera y Cambio Climático, Universidad Nacional, Mexico City, 04510, Mexico
[3]Departamento de Sistemas Físicos, Químicos y Naturales, Universidad Pablo de Olavide, Sevilla, Spain
[4]Karlsruhe Institute of Technology, Institute for Meteorology and Climate Research, Hermann-von-Helmholtz-Platz 1, 76344 Leopoldshafen, Germany
[5]Istituto di Fisica Applicata "Nello Carrara" (IFAC) del Consiglio Nazionale delle Ricerche (CNR), Florence, Italy
[6]University of Toronto, Department of Physics, 60 St. George Street, Toronto, Ontario M5S1A7, Canada
[7] Instituto de Estructura de la Materia, CSIC, Serrano 121 28006, Madrid, Spain

Correspondence to: P.Ordoñez L. Acosta (p.ordonez.perezacosta@gmail.comfisica.unam.mx)

Abstract. Variations in the isotopologicál composition of water vapour are fundamental for understanding the relative importance of different mechanisms of water vapor transport from the tropical upper troposphere to the lower stratosphere. Previous comparisons obtained from observations of H_2O and HDO by satellite instruments showed discrepancies. In this work, newer versions of H_2O and HDO retrievals from Envisat/MIPAS and SCISAT/ACE-FTS are compared with data derived from SCISAT/ACE-FTS. Specifically, MIPAS-IMK V5, MIPAS-ESA V8, and ACE-FTS V4.1/4.2 for the common period from February 2004 to April 2012 are compared for the first time through a profile-to-profile approach and comparison based on climatological structures. The comparison is essential for the scientific community to assess the quality of new satellite data products, a necessary procedure to validate further scientific work. Stratospheric H_2O and HDO global average coincident profiles analysis reveal good agreement between 16 km and 30 kmThe smallest biases are found between 20 and 30 km, and the largest biases are exhibited around 40 km both in absolute and relative terms. For HDO, biases between -8.6 10.6 % are observed among the three databases in the altitudes of 16 to 30 km. However, around 40 km, ACE-FTS agrees better to MIPAS-IMK than MIPAS-ESA, with biases of -4.8% and -37.5%, respectively. For HDO bias between MIPAS-IMK and MIPAS-ESA is 28.1 % at this altitude. For HDO and δD, lower biases are found in the MIPAS-ESA and ACE-FTS comparison, even if associated to a larger de-biased standard deviation. The meridional cross-sections of H_2O and HDO exhibit the expected distribution that has been established in previous studies. For δD the tropical depletion in ACE-FTS and MIPAS-ESA occurs on the top of the dynamical tropopause, but this minimum is found at higher altitudes in MIPAS-IMK dataset. The tape recorder signal is present in H_2O and HDO for the three databases with slight quantitative differences. The δD annual variation for ACE-FTS data and MIPAS-ESA data is very weak compared to the MIPAS-IMK dataset, which shows a coherent tape recorder signal clearly detectable up to at least 30 km. The observed differences in the climatological δD composites between databases

could lead to different interpretations regarding the water vapor transport processes toward the stratosphere. Therefore, it is important to further improve the quality of Level 2 products.

1. INTRODUCTION

Water vapour (WV) is the most important non-anthropogenic greenhouse gas in Earth's atmosphere (Hegglin et al., 2014). Although WV concentration is much lower in the stratosphere than in the troposphere, it significantly affects the climate at the surface (Solomon et al., 2007). Stratospheric water vapour (SWV) affects atmospheric dynamics and thermodynamics by modulating the radiative forcing directly (e.g., Solomon et al., 2010; Riese et al., 2012) and indirectly through its effect on the stratospheric ozone chemistry (Vogel et al., 2011). Moreover, it has been shown that the cold point temperature in the tropics is expected to rise in the future which will lead to increasing SWV due to reduced freeze-drying in the tropical tropopause layer (TTL; Gettelman et al., 2009). This implies the existence of a SWV feedback (Dessler et al., 2013; Banerjee et al., 2020).

The humidity in the lower stratosphere has been increasing in the last decades. Scientists discovered it at the beginning of the century. However, the reason for this humidification was not understood (Rosenlof et al., 2001). Because of the number of atmospheric composition measurement instruments that have been implemented on satellites over the past several decades, studies related to the SWV transport process have been increasing (e.g., Mote et al., 1996; Steinwagner et al., 2007; Lossow et al., 2011; Randel et al., 2012; Scheepmaker et al., 2016; Schneider et al., 2020). Brewer-Dobson circulation (Brewer, 1949) transports H_2O-rich air through upwelling from low tropospheric latitudes, accompanied by large horizontal motions to mid-stratospheric latitudes. WV is also produced in the middle atmosphere through methane oxidation and is destroyed through photodissociation and reactions with O(1D) (Wang et al., 2018). However, the observed variability in SWV concentrations cannot be fully explained by observed changes in these main drivers (Hegglin et al., 2014). Therefore, studies focused on the dynamical processes that determine SWV variability constitute an active contemporary area of research (Plaza et al., 2021).

One way to conduct studies of troposphere-stratosphere mass transport is through isotopologues related to these species that behave as phenomenological tracers (Kuang et al., 2003). The isotopologic~~al~~ composition of WV molecules in the stratosphere provides an observational constraint for determining the relative importance of the possible transport mechanisms (Payne et al., 2007). Among the isotopologuesical species of WV, $HD^{16}O$ (hereafter HDO) is particularly useful due to its significant fractionation effect (Merlivat and Nief, 1967; Kuang et al., 2003). Therefore, the analysis of HDO at the tropopause is a very useful tracer to diagnose the relative importance of slow ascent and convective ice-lofting for WV transport into the stratosphere (Moyer et al., 1996; Tuinenburg et al., 2015; Wang et al., 2019).

Satellite remote sounding of the Earth's limb is currently the only method of ~~observing the atmosphere that allows~~providing near-global time series of atmospheric profiles ~~to be obtained~~ from the upper troposphere to the lower thermosphere (Sheese

et al., 2017). However, each atmospheric measurement with this method has its sources of uncertainty and systematic biases, which must be examined. Limb earth probing instruments may exhibit other systematic differences from similar devices depending on the observed latitudinal region and/or the observed local time. In addition to the differences due to each molecule's volume mixing ratio (VMR) retrieval algorithms, these biases must also be characterized. Sometimes, even significant discrepancies between data retrieved from the same satellite can be found depending on the algorithm.

There are different datasets of WV and its isotopologues in the stratospheric region, retrieved mainly from three instruments. One of them, the Odin satellite, carries a Sub-Millimetre Radiometer (SMR), observing stratospheric H_2O, $H_2{}^{18}O$, and HDO (Murtagh et al., 2002). For technical reasons (the maximum bandwidth of a single radiometer is only 0.8 GHz), ~~and~~ H_2O and HDO cannot be measured simultaneously (Wang et al., 2018). Therefore, this study is focused on the other two instruments.

The instrument MIPAS (Michelson Interferometer for Passive Atmospheric Sounding; Fischer et al., 2008) aboard Envisat (Environmental Satellite) was launched in 2002 and ceased operation in 2012 ~~when contact with the satellite was lost~~. This instrument makes highly reliable WV observations in the stratosphere (Payne et al., 2007; von Clarmann et al., 2009; Ceccherini et al., 2011; Kiefer et al., 2023). On the other hand, the instrument ACE-FTS (Atmospheric Chemistry Experiment - Fourier Transform Spectrometer; Bernath et al., 2005; Nassar et al., 2005) that yields WV information in the stratosphere to the present day (Boone et al., 2020) is aboard the Canadian satellite SCISAT, which was launched in 2003.

In the case of MIPAS, different retrieval~~s~~ methods have been developed. One of the data sets, named here MIPAS-IMK, was retrieved with the IMK/IAA processor, which was developed in collaboration between the "Institut für Meteorologie und Klimaforschung" (IMK) in Karlsruhe, Germany, and the "Instituto de Astrofísica de Andalucía" (IAA) in Granada, Spain (~~see for general description, e.g., Högberg et al., 2019; Lossow et al., 2019; Lossow et al., 2020; Hegglin et al., 2013~~ Speidel et al., 2018). The other MIPAS dataset, named here MIPAS-ESA V8 products (Dinelli et al. 2021), was retrieved by using the Optimized Retrieval Model (ORM) algorithm (Raspollini et al., 2022 and references therein) on the full-mission reprocessing campaign performed on L1V8 (Kleinert et al., 2018). The ACE-FTS retrievals have evolved through several versions with the retrieval model being updated with optimized parameters (Boone et al., 2005, 2013, 2020). In this work, we evaluate H_2O and HDO data sets derived from level-1b version 5 observations by MIPAS-IMK ~~V5H and V5R~~, MIPAS-ESA ~~level 2~~ V8.0, and ACE-FTS V4.1/4.2 for the common period from February 2004 to April 2012.

WV observations have been collectively evaluated through a multitude of parameters, like biases, drifts or variability characteristics, correlations, and other statistical data by the WCRP/SPARC water vapor assessment II (WAVAS-II) activity (https://amt.copernicus.org/articles/special_issue10_830.html). The last evaluation of Lossow et al. (2019) used ACE-FTS v3.5 (2004-2014), MIPAS-ESA V6 version (2002-2012) and V7 version (2005-2012), ~~V5H (2002-2004), and MIPAS-ESA V7R (2005-2012),~~ MIPAS-IMK V5H H2O 20 (2002-2004) ~~version 20~~ and V5R H2O 220/221 (2005-2012) ~~version 220/221~~.

In this work, we use newer versions of some H_2O data sets than those employed in the previous studies, including MIPAS-ESA v8 and ACE-FTS V~~v~~4.1/4.2, whose improvements will be described in the next section.

Regarding HDO, Lossow et al. (2011) compared V5H_HDO_20 (2002-2004) ~~data from MIPAS Level 1~~ retrieved with the IMK/IAA processor ~~(data version 20)~~, SMR ~~from~~ / Odin version 2.1, and ACE-FTS version 2.2, and they found good general agreement. However, distinct observational discrepancies of the δD (see section 3.2) annual variation were visible between MIPAS-IMK (Steinwagner et al., 2010) and ACE-FTS (Randel et al., 2012) data. Högberg et al (2019) assessed the profile-to-profile comparisons of stratospheric δD using two MIPAS-IMK sets from the retrieval based on V5H_H2O/HDO_20 and ACE-FTS V2.2 and V3.5. The overlap period was very limited, from February 2004 to March 2004. During this short overlap period, the majority of ACE-FTS observations occurred in March at northern polar latitudes and most of the coincidences are concentrated near 70º N. ~~V2.2 and~~ Lossow et al. (2020) reassessed the discrepancies in the annual variation δD in the tropical lower stratosphere based on MIPAS-IMK and ACE-FTS data sets. Overall, the ~~used~~ data set utilized covered the period from July 2002 to March 2004, which is referred to as the full resolution period of MIPAS ~~(Lossow et al., 2020)~~. However, a longer time series is needed to draw robust conclusions on the relative importance of different mechanisms transporting WV into the stratosphere. ~~Therefore, we focus here on newer data versions that cover the full mission period of ten years.~~ Therefore, we use a new HDO data version called MIPAS-IMK_V5H_HDO_22 (2002-2004) and VR5_HDO_222/223 (2005-2012) that ~~These data versions~~ were first published by Speidel et al. (2018) ~~and not yet been compared to other observations~~. For HDO MIPAS-ESA, there are no published comparisons yet. We focus here on the overlap period between MIPAS and ACE-FTS which is from 2004 to 2012.

We compare the three H_2O, ~~and~~ HDO and δD ~~observation~~ databases relying on two approaches. First, we present profile-to-profile comparisons and provide a general overview of the typical biases in the observational databases. The second approach is based on climatological comparisons, including meridional cross sections and time series comparisons. Section 2 describes the individual data sets in detail. In section 3, the methodology is outlined. Section 4 presents the results, which will be summarised in section 5.

2. DATA SETS

As mentioned in the introduction, with the only exception of MIPAS-IMK H_2O data, which use MIPAS-IMK V5H_H2O_20 (2002-2004) and V5R_H2O_220/221 (2005-2012) as in Lossow et al., 2019, we employ newer data sets than those used in the previous studies. Here, we employ ~~the MIPAS-IMK V5H_H2O_20 (2002-2004) and V5R_H2O_220/221 (2005-2012) for H_2O case, and~~ MIPAS-IMK V5H_HDO_22 (2002-2004) and V5R_HDO_222/223 (2005-2012) for HDO (Speidel et al., 2018), the MIPAS ESA Level 2 V8 dataset (Dinelli et al., 2021) results from the full-mission reprocessing campaign performed on L1V8 products and ACE-FTS V~~v~~4.1/v.2 (Boone et al., 2020) for both isotopologues.

2.1. MIPAS

MIPAS was a cooled, high-resolution Fourier transform spectrometer aboard Envisat (Fischer et al., 2008). Envisat was launched on 1 March 2002 and made observations until 8 April 2012, when communication with the satellite was lost. Envisat orbited the Earth 14 times a day in a sun-synchronous polar orbit at about 790 km altitude inclined of 98.55 with respect to the plane of the Equator. The equator crossing times were 10:00 and 22:00 local time for the descending and ascending nodes, respectively. MIPAS measured the thermal emission of the atmospheric limb, covering all latitudes. MIPAS operated at 100 % of its duty cycle from July 2002 to March 2004, when, due to a significant anomaly affecting the Interferometer Drive Unit (IDU), its regular operations were interrupted to avoid the mechanical blockage of the instrument (Dinelli et al., 2021). After various tests with different spectral resolutions, the European Space Agency (ESA) recovered the instrument in January 2005 at a reduced spectral resolution but a finer vertical sampling. At the beginning of 2005, MIPAS operated at only a 30-% duty cycle, which progressively increased until December 2007, when it was successfully restored to 100% operations (Kleinert et al., 2007, 2018). MIPAS operated in several observation modes regarding the altitude range covered and the width of the tangent altitude grid. Of relevance here are only the NOM (~5 to 72 km), ~~several~~ UTLS-1 (~5 to 49 km), and the Aircraft emission (~7 to 38 km) observation modes.

2.1.1. MIPAS-~~ESA~~~~IMK~~

The MIPAS ESA Level 2 V8 dataset (Dinelli et al., 2021) results from the full-mission reprocessing campaign performed on L1V8 products using the Optimized Retrieval Model (ORM) processor version 8.22 (Raspollini et al., 2022) funded by the European Space Agency (ESA). As a general approach, the retrieval algorithm fits modelled spectra to measured infrared spectra in species-dependent micro-windows via least-squares global fitting. For iteration control, the Gauss-Newton approach modified with the Levenberg-Marquardt method is used to minimize the fit residuals. Within the retrieval of data from the second phase of MIPAS operation, regulation is needed because the tangent altitude steps were smaller than the field-of-view width so that the spectra along a vertical profile were not independent, and the inversion problem was underdetermined for retrieval of a value at each tangent height. The regularization is applied a posteriori in case of H_2O with a retrieval error-dependent regularisation strength (Ridolfi and Sgheri, 2011). HDO was retrieved for the first time within the V8 data set. The retrieval is set up as optimal estimation retrieval. The a priori used is the previously retrieved H_2O profile, scaled by the constant isotopic ratio used by the HITRAN spectroscopic database VSMOW (see Sect.3). The diagonal elements of the covariance matrix of the a priori which determine the strength of the regularization~~,~~ are computed as the square of the sum of a constant (10^{-3} ppmv) plus the 100% of the a priori profile. This choice assures that the assumed uncertainty of the a priori is at least 100% of the a priori profile or 1 ppbv squared, whatever is larger, to keep the regularization strength low. The non-diagonal elements are computed assuming a correlation length of 10 km in the vertical. HDO has been retrieved from all the observation modes listed above; the useful altitude range is reported to be 5 to 55 km (Raspollini et al., 2021). The

microwindows used for the retrieval of HDO lie in the 1218 cm^{-1} to 1471 cm^{-1} spectral range, while the ones used for the retrieval of H_2O lies in the ranges 783 to 956 cm^{-1} and 1224 to1696 cm^{-1}.

MIPAS ESA L2 analysis uses the HITRAN_mipas_pf4.45 spectroscopic database. It is based on HITRAN08 (Rothman et al., 2009), but spectroscopic parameters for the molecules H_2O, O_2, SO_2, OCS, CH_3Cl, C_2H_2 and C_2H_6 are taken from HITRAN 2012 (Rothman et al., 2012). The spectroscopic parameters of HNO_3 were derived by Perrin et al. (2016), and the spectroscopic data for COCl2 were derived by Tchana et al. (2015). Both HNO_3 and $COCl_2$ data are now contained in HITRAN 2016 (Gordon et al., 2017).

The estimation of the systematic error of MIPAS-ESA H_2O and HDO profiled can be found at http://eodg.atm.ox.ac.uk/MIPAS/err/err_hdo_day_or27.png and http://eodg.atm.ox.ac.uk/MIPAS/err/err_h2o_day_or27.png respectively. Noise error, Averaging Kernels, vertical resolution are discussed at https://earth.esa.int/eogateway/documents/20142/37627/README_V8_issue_1.1_20210916.pdf.

H_2O vertical resolution is about 3 at 10 km, then it slowly degrades, reaching 5 - 6 km at 20 km, 7.5 at 30 - 40 km, 10 at 50 km. The total random error is about 1-2% in the range 50 hPa-1 hPa for all atmospheres except polar winter, where it may reach values even larger than 5%. The tropopause is characterized by large percent random noise (also due to the minimum of the VMR), in the mesosphere random error rapidly increases with the altitude. HDO vertical resolution is 3-3.5 km in the range 6-10 km, about 5 km in the range 6-30 km, it is 7.5 km at 40 km and 12.5 km at 50 km. The relative average single scan random error varies with altitude for the different atmospheres, but it is never smaller than 25%.

~~MIPAS-IMK database is obtained from the collaboration between IMK and IAA with the algorithm that they developed for the retrieval of VMR that produces level 2 data (von Clarmann et al., 2009). The IMK-IAA algorithm uses a non-linear least-squares global-fitting technique with Tikhonov regularisation, which is a constrained iterative inversion technique. Small spectral regions, so-called microwindows, are used where the respective species have suitable spectral lines. The data are retrieved on a 1-km grid, and the efficiency-dependent strength of the smoothing constraint was chosen to optimize vertical resolution while limiting unphysical oscillations in the retrieved profile. MIPAS-IMK-WV retrievals are performed in $\log(VMR)$ space (see e.g., the SPARC-WAVAS-II Special issue (https://amt.copernicus.org/articles/special_issue10_830.html) for validation of this data version. The HDO data version used here differs significantly from the data versions assessed by Lossow et al. (2020) and Högberg et al. (2019) and used by Steinwagner et al. (2007, 2010). For the data version used here, HDO was retrieved in linear space with the previously retrieved main isotopologue profile as a priori information. δD (see section 3.2) is calculated from the regular water vapour product and HDO; by this the disadvantage of using a less-than-optimal data version of H_2O is omitted, and the vertical resolution of δD is provided by the difference of the a priori and retrieved profile (Speidel et al., 2018).~~

2.1.2. MIPAS-IMK~~ESA~~

The MIPAS-IMK database is a product of the collaboration between IMK and IAA who developed an algorithm for the retrieval of the VMR of about 30 different trace gases from MIPAS level-1b data independent of the ESA algorithm (von Clarmann et al., 2009). Similar to the MIPAS-ESA product, the IMK-IAA algorithm uses a non-linear least-squares global-fitting technique with Levenberg-Marquardt damping to fit simulated spectra to measured ones within spectral microwindows where the respective species have suitable spectral lines. In contrast to the MIPAS-ESA approach whose retrieval grid coincides with the tangent altitudes of the measurements, the level-2 data are retrieved on a fixed grid of 1 km ~~grid~~step ~~with~~ up to 46 km and 2 km above. This grid width again requires regularization to stabilize the retrieval. A Tikhonov regularization was chosen that acts as a smoothing constraint by weighted minimization of the squared first order finite differences of adjacent profile values. The regularization strength was chosen to optimize vertical resolution while limiting unphysical oscillations in the retrieved profiles. The MIPAS-IMK WV retrievals used here were retrieved in log (VMR) space from V5 MIPAS spectra (see e.g., the SPARC-WAVAS-II Special issue (https://amt.copernicus.org/articles/special_issue10_830.html for validation of this data version, V5H_H2O_20 and V5R_H2O_220/221). The HDO data version used in this study differs significantly from the data versions assessed by Lossow et al. (2020) and Högberg et al. (2019) and used by Steinwagner et al. (2007, 2010). For the data version used here (V5H_HDO_22 and V5R_HDO_222/223), HDO was retrieved in linear space with the previously retrieved main isotopologue profile, scaled by the constant isotopic ratio used in the HITRAN database (VSMOW) as a priori information. δD (see section 3.2) is calculated from the regular water vapour product and HDO; by this new approach the disadvantage of using a less-than-optimal data version of H_2O is omitted, and the vertical resolution of δD is provided by the difference between the a priori and the retrieved profile (Speidel et al., 2018). By this change of the retrieval approach the disadvantages of the previous HDO and δD data product demonstrated by Lossow et al. (2020) should be overcome. MIPAS-IMK V5H_HDO_22 (2002-2004) and V5R_HDO_222/223 (2005-2012) data are available from NOM observation mode only, leading to a lower number of total available profiles than for ESA data. Spectral microwindows in the 1250 to 1482 cm^{-1} range were used for the HDO retrieval while H_2O was retrieved in the 795 to 827 cm^{-1} and 1224 to 1410 cm^{-1} spectral range. Spectroscopic data from the MIPAS-specific data base MIPAS_pf3.32 were used, which are, for H2O and HDO, essentially the same data as in its earlier version published by Flaud et al. (2003) and based in general on the HITRAN1996 data base (Rothman et al., 1998). Differences for H_2O and HDO between MIPAS pf3.32 and HITRAN1996 are updates that were available at the HITRAN web site at the time when the MIPAS-specific data base was collected, and parameters for the main isotopologue derived from recent theoretical calculations (for more details, see Flaud et al. (2003)).

Information on systematic errors, averaging kernels and vertical resolution of H2O can be found in von Clarmann et al., 2009. In summary, the vertical resolution is between 2.3 km in the lower and 6.9 km in the upper stratosphere. The systematic errors are dominated by spectroscopic uncertainties and are in the order of 7 to 19%. For HDO, the estimated random errors are between 15% at about 15 km and 35% at 40 km altitude, and the vertical resolution increases from 3 to 4 km up to 25km to 6

km at 35 km. The averaging kernels are well behaved, i.e. peak at the nominal retrieval height, between 15 and 40 km. The systematic errors are again dominated by spectroscopic uncertainties.

~~The MIPAS ESA Level 2 V8 dataset (Dinelli et al., 2021) results from the full-mission reprocessing campaign performed on L1V8 products using the Optimized Retrieval Model (ORM) processor version 8.22 (Raspollini et al., 2022) funded by the European Space Agency (ESA). The algorithm fits forward-model spectra to measured infrared spectra in species-dependent micro-windows via least-squares global fitting, using the Gauss-Newton approach modified with the Levenberg-Marquardt method to minimize the fit residual. For H_2O a posteriori regularisation is applied with a retrieval error-dependent regularisation strength (Ridolfi and Sgheri, 2011). For HDO, retrieval is performed with Optimal Estimation, with the a priori profile equal to the retrieved H_2O profile, opportunely scaled according to the constant value of the HDO isotopic abundance (3.107×10^{-4}), provided by the HITRAN spectroscopic database. The diagonal elements of the covariance matrix of the a priori are computed as the square of the sum of a constant (10^{-3} ppmv) plus the 100% of the a priori profile, while the non-diagonal elements are computed assuming a correlation length of 10 km. The forward model used in the algorithm accounts for horizontal inhomogeneities of temperature and trace species and assumes that the atmosphere is in local thermodynamic equilibrium (LTE).~~

2.2. ACE-FTS

ACE-FTS is one of three instruments aboard the Canadian satellite SCISAT (Bernath et al., 2005). SCISAT was launched on the 12 August 2003 into a highly inclined, 74°, orbit at 650 km altitude. This orbit provides latitudinal coverage of 85° S to 85° N but is optimized for observations at high and middle latitudes. ACE-FTS measures the Earth's atmosphere during up to 15 sunrises and 15 sunsets daily, from approximately 5 to 150 km altitude. Vertical sampling varies with altitude and orbit beta angle, from a minimum of around 1 to 2 km in the upper troposphere up to a maximum of approximately 6 km in the upper stratosphere and mesosphere. HDO information is retrieved from two spectral bands: 3.7 to 4.0 µm (2493-2673 cm^{-1}) and 6.6 to 7.2 µm (1383-1511 cm^{-1}). H_2O retrieval uses spectral information between 3.2 and 10.7 µm (937-3173 cm^{-1}) (Boone et al., 2005).

Here, we use ACE-FTS version 4.1/4.2. The ACE-FTS trace species VMR retrieval algorithm is described by Boone et al. (2005, 2013), and the changes for the version 4.1/4.2 retrieval are provided in Boone et al. (2020). Similar to MIPAS, the retrieval algorithm uses a non-linear least-squares global-fitting technique that fits forward modelled spectra to the ACE-FTS observed spectra in given microwindows - based on line strengths and line widths from the HITRAN 2016 database (with updates as described by Gordon et al. (2017)). The pressure and temperature profiles used in the forward model are the ACE-FTS derived profiles, calculated by fitting CO_2 lines in the observed spectra. The version 4.1/4.2 retrieval grid uses a minimum altitude spacing of 2 km for tangent heights above 15 km and a minimum spacing of 1 km for tangent heights below 15 km. This limitation on the retrieval grid suppresses unphysical oscillations that commonly occurred above 15 km in previous

processing versions when the tangent height spacing dropped below 2 km. The main changes made in the v4 retrievals are updated micro windows for most species that allow for a more significant number of interfering species; improvements to the temperature and pressure retrievals, leading to fewer unnatural oscillations in the vertical profiles (Sheese et al., 2017). ~~ACE-FTS is one of three instruments aboard the Canadian satellite SCISAT (Bernath et al., 2005). SCISAT was launched on the 12 August 2003 into a highly inclined, 74°, orbit at 650 km altitude. This orbit provides latitudinal coverage of 85° S to 85° N but is optimized for observations at high and middle latitudes. ACE-FTS scans the Earth's atmosphere during up to 15 sunrises and 15 sunsets daily from approximately 5 to 150 km altitude. Vertical sampling varies with altitude and orbit beta angle, from around 1 to 2 km in the upper troposphere through approximately 6 km in the upper stratosphere and mesosphere. HDO information is retrieved from two spectral bands: 3.7 to 4.0 µm (2493-2673 cm^{-1}) and 6.6 to 7.2 µm (1383-1511 cm^{-1}). H_2O retrieval uses spectral information between 3.3 and 10.7 µm (937-2993 cm^{-1}) (Lossow et al., 2020). Here, we use ACE-FTS version 4.1/4.2. The ACE-FTS trace species VMR retrieval algorithm is described by Boone et al. (2005, 2013), and the changes for the most recent version of the retrieval v4.1/4.2 are Boone et al. (2020). The retrieval algorithm uses a non-linear least-squares global-fitting technique that fits the ACE-FTS observed spectra in given micro- windows to forward modelled spectra based on line strengths and line widths from the HITRAN 2016 database (with updates as described by Gordon et al. (2017)). The pressure and temperature profiles used in the forward model are the ACE-FTS derived profiles, calculated by fitting CO_2 lines in the observed spectra. The version 4.1/4.2 retrieval grid uses a minimum altitude spacing of 2 km for tangent heights above 15 km and a minimum spacing of 1 km for tangent heights below 15 km. This limitation on the retrieval grid suppresses unphysical oscillations that commonly occurred above 15 km in previous processing versions when the tangent height spacing dropped below 2 km. The main changes made in the v4 retrievals are amended micro windows for most species that allow for a more significant number of interfering species; improvements to the temperature and pressure retrievals, leading to fewer unnatural oscillations in the vertical profiles (Sheese et al., 2017).~~

3. METHODS

All data used here were managed in agreement with the user manuals of each dataset. For MIPAS-IMK, we followed Lossow et al. (2020) and Högberg et al. (2019). For ACE-FTS, we used the specifications given by Sheese et al. (2015) and Boone et al. (2020), and Dinelli et al. (2021) was employed for MIPAS-ESA. The present quality assessment of H_2O, ~~and~~ HDO and δD data mainly focuses on the stratosphere, although data for the upper troposphere and lower mesosphere are used if available. ~~The data quality assessment process is performed for H_2O and HDO from the three databases.~~

For calculating δD~~Using the results of the procedure described before~~, we assessed the isotopic composition through the expression $R = \frac{[D]}{[H]}$ that can be determined through the concentration of the isotopologues of water as follows:

$$R = \frac{[\mathrm{D}]}{[\mathrm{H}]} = \frac{[\mathrm{HDO}] + 2[\mathrm{DDO}]}{2[\mathrm{H_2O}] + [\mathrm{HDO}]} \approx \frac{[\mathrm{HDO}]}{2[\mathrm{H_2O}]} \quad (1)$$

To quantify the abundances of heavy isotopes, R is usually compared to a standard reference ratio known as R_{VSMOW} through the following relationship:

$$\delta D = \left(\frac{R}{R_{VSMOW}} - 1\right) \times 1000 \quad (2)$$

where VSMOW=155.76 x 10^{-6} is the reference ratio (Vienna Standard Mean Ocean Water; Hagemann et al., 1970).

3.1. Profile to profile comparisons

This approach is based on the comparison of averages of coincident profiles. ~~We use the profile-to-profile comparison approach proposed by Högberg et al. (2019), where each profile was interpolated on a common regular altitude grid, defined as the height vector of MIPAS-IMK from 1 to 70 km.~~

~~3.1.1 Coincidences~~

For the ~~final~~ coincidence pairs, the ACE-FTS data, which is the sparser dataset in the tropics was used as the first data set. Then, ACE-FTS and MIPAS-ESA~~global~~ observations are considered to be coincident when they meet the following criteria (Högberg et al., 2019):

- Spatial separation of less than 1000 km.
- Temporal separation less than 24 h.
- Geolocation separation less than 5º, both in longitude and equivalent latitude.

The MIPAS-IMK profile ~~closes~~coincident~~t to~~with the selected MIPAS-ESA profile was found by using the following criteria:

- Temporal separation less or equal to 2 seconds.
- Geolocation separation less than 1º, both in latitude. ~~For the final coincidence pairs, the ACE-FTS data, which is the sparser dataset was used as the first data set in all comparisons to avoid inconsistent results.~~
-

Figure 1 shows a map for all ~~ACE-FTS and MIPAS-IMK~~ the coincident profiles ~~(Fig. 1(a)) and ACE-FTS and MIPAS-ESA coincident profiles (Fig. 1(b))~~ between 25-27 July 2010, illustrating ~~. Figure 1 illustrates~~ that for each ACE-FTS profile (green~~black~~ diamond~~circles~~), there is ~~two or three~~one MIPAS-IMK (red~~blue~~ square~~crosses~~) and one MIPAS-ESA (blue~~red~~ asterisk~~crosses~~) profile~~s~~ that meet the coincidence criteria. Only data points with the full triple of observations (ACE-FTS, MIPAS-ESA, and MIPAS-IMK) were used for direct comparisons described below. ~~This is because the horizontal difference between two MIPAS profiles is appr. 400 km, i.e., two to three profiles fall into the coincidence radius. The corresponding values are arithmetically averaged if multiple coincidences are found in coincident regions, generating a single point. One observation from ACE can be found to be coincident with other MIPAS observations. In the comparisons between MIPAS instrument databases, we have chosen MIPAS-ESA as the reference database. It should be mentioned that the coincident~~

profiles from ESA and IMK are not necessarily the same because of profiles potentially not available due to convergence issues in the retrieval, or due to flags filtering out different profiles.

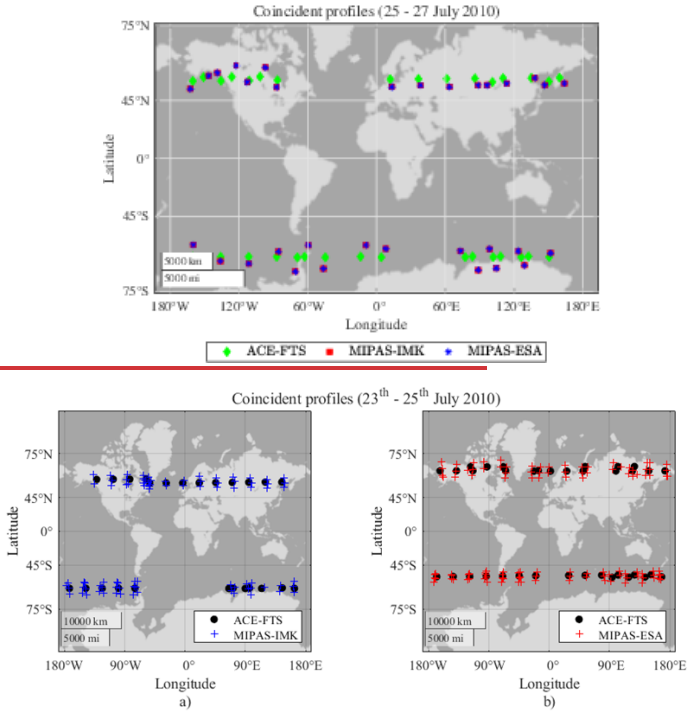

Figure 1. Coincident profiles between ~~(a)~~ ACE-FTS, MIPAS-ESA and MIPAS-IMK ~~and (b) ACE-FTS and MIPAS-ESA~~ on 25-27 July 2010. Different markers indicate the database, ACE-FTS (green diamonds~~black circles~~), MIPAS-IMK (red squares~~blue crosses~~), and MIPAS-ESA (blue asterisks~~red crosses~~). ~~The profiles from each dataset were linearly interpolated for the comparisons onto a 58 levels grid between 0 to 70 km, which are the altitude reference levels of MIPAS-IMK as described by Lossow et al. (2011).~~

~~3.1.2. Comparison of vertical profiles~~

The profiles from each dataset were linearly interpolated for the comparisons onto a 58 levels grid from~~between~~ 10 to 70 km (1-km grid from 0 to 44 km, followed by a 2-km step width from 46 to 70 km), which are the altitude reference levels of MIPAS-IMK as described by Lossow et al. (2011). ~~Once the orbits of the coincident profiles have been obtained, the global average altitude profiles are determined.~~ Fig. 2 ~~(a) and Fig. 2(b)~~ shows the number of matched profiles by altitude between

ACE-FTS, MIPAS-ESA and MIPAS-IMK. ~~and, ACE-FTS and MIPAS-ESA, respectively. However, i~~It ~~is crucial to exercise caution when interpreting these results~~ found here, ~~specifically considering the sampling limitations of ACE-FTS in the tropics (Randel et al, 2012), during the period of study, especially at lower altitudes. In both cases,~~ T~~t~~he number of valid matches increases in the UTLS, and more than 140,000 matched profiles are obtained from the mid-stratosphere ~~and upwards~~. The number of ACE-FTS HDO profiles decreases from 40 km of altitude and upwards. At 48 km of altitude the last profile is found.

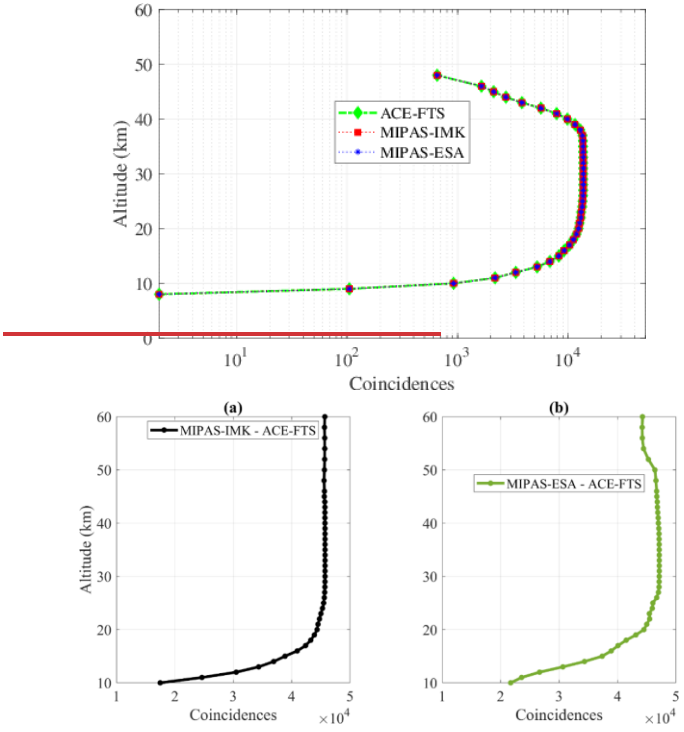

Figure 2. The ~~global~~ number of coincident sets of data (2004-2012) for ~~(a) MIPAS-IMK and~~ ACE-FTS, ~~and (b)~~ MIPAS-ESA and MIPAS-IMK ~~ACE-FTS~~ comparisons.

Then, the mean is computed as the arithmetical average of the data distribution for each altitude level and the data dispersion is obtained by the standard error of the mean~~deviation~~. δD can be quantified by two approaches: (1) calculate R from individual HDO and H_2O profiles and average the results, or (2) first compute the averages values of H_2O and HDO from all the profiles and then calculate R. In this work, the second approach is used as defined by Högberg et al. (2019): the results are derived separately for HDO and H_2O and after this, combined to δD as Högberg et al. (2019) and Lossow et al (2020).

3.1.~~1~~3. Bias determination

Four statistical parameters have been calculated ~~for the globe~~ globally at each altitude level: mean absolute biases, mean relative biases, the de-biased standard deviation of the relative biases, and Pearson correlation coefficient ~~for three of the six possible comparisons in pairs of data~~. ~~These evaluations follow the methodology used in previous assessments (Lossow et al., 2019, Högberg et al., 2019, Wetzel et al., 2013) and follow the recommendations of Loew et al. (2017).~~ ~~**(a) The mean absolute bias:**~~ Tthe mean bias between two coincident data sets for a specific altitude level ~~and for a given isotopologue I (i.e., HDO, H_2O),~~ has been calculated as:

$$\bar{b}(z) = \frac{1}{n(z)} \sum_{i=1}^{n(z)} \delta_i(z) \qquad (3)$$

where n denotes the corresponding number of coincident measurements, ~~θ the latitude,~~ and z the altitude, ~~t the period and $b_i(I, \theta, z, t)$ are the individual differences between them~~. These differences are considered as:

$$\delta_i(z) = \frac{x_i(z)_1 - x_i(z)_2}{x_i(z)_{ref}} \qquad (4)$$

where $x_i(I, \theta, z, t)_1$ are the individual H_2O, ~~or~~ HDO or δD abundances of the first data set and $x_i(I, \theta, z, t)_2$ are the abundances of the second data set that are compared.

The mean absolute bias:

this is calculated when $x_i(z)_{ref} = 1$ for absolute analysis in Eq. (4)

$$\overline{b_{abs}}(~~I, \theta,~~ z~~, t~~) = \frac{1}{n(z)} \sum_{i=1}^{n(z)} x_i(z)_1 - x_i(z)_2 \frac{~~1~~}{~~n~~} \sum_{i=1}^{~~n~~} ~~b_i(I, \theta, z, t)~~ \qquad (5~~3~~)$$

~~where n denotes the corresponding number of coincident measurements, θ the latitude, z the altitude, t the period and $b_t(I,\theta,z,t)$ are the individual differences between them. These differences are considered as:~~

~~$$b_t(I,\theta,z,t) = x_t(I,\theta,z,t)_1 - x_t(I,\theta,z,t)_2 \quad (2)$$~~

~~where $x_t(I,\theta,z,t)_1$ are the individual H_2O or HDO or δD abundances of the first data set and $x_t(I,\theta,z,t)_2$ are the abundances of the second data set that are compared.~~

~~(b)~~The mean relative bias:

T~~t~~his is calculated by dividing the mean absolute bias by the mean reference value (Wetzel et al., 2013).

~~$$\overline{b_{rel}}(I,\theta,z,t) = \frac{\overline{b_{abs}}(I,\theta,z,t)}{\frac{1}{n}\sum_{i=1}^{n} x_{ref}(I,\theta,z,t)}; \quad (3)$$~~For the reference value, different options are possible (e.g., Randall et al., 2003; Dupuy et al., 2009). The mean of the two datasets have been chosen because the satellite observations can have large uncertainties, and thus the mean is an appropriate approach (Lossow et al., 2019):

$$x_{i_{ref}}(I,\theta,z,t) = \frac{x_i(I,\theta,z,t)_1 + x_i(I,\theta,z,t)_2)}{2} \quad (6)$$

Then, considering the Eq. (3) and (4) the mean relative bias is given by:

$$\overline{b_{rel}}(z) = \frac{1}{n(z)} \sum_{i=1}^{n(z)} 2\left(\frac{x_i(z)_1 - x_i(z)_2}{x_i(z)_1 + x_i(z)_2}\right) \quad (7~~5~~)$$

~~(c)~~ De-biased standard deviation:

The de-biased standard deviation ($\sigma_{\overline{b}}$) is represented by the standard deviation of the mean relative bias-corrected between the two sets of compared data:

$$\sigma_{\overline{b}}(I,\theta,z,t) = \sqrt{\frac{1}{n(z)-1}\sum_{i=1}^{n}\left(\delta b_i(I,\theta,z,t) - \overline{b(I,\theta,z,t)}\right)^2} \quad (8~~6~~)$$

This quantity measures the precision of the relative bias between the two datasets being compared, particularly in cases where a complete evaluation of the random error budget is not available for all the instruments involved (von Clarmann et al., 2006).

~~(d)~~ **Pearson correlation coefficient:**

The correlation coefficient r dependent on altitude levels is defined as:

$$r(\sout{I,\theta,z,t}) = \frac{1}{n(z)-1}\sum_{i=1}^{n(z)}\left(\frac{x_i(\sout{I,\theta,z,t})_1 - \overline{x(\sout{I,\theta,z,t})_1}}{\sigma_{x_1}}\right)\left(\frac{x_i(\sout{I,\theta,z,t})_2 - \overline{x(\sout{I,\theta,z,t})_2}}{\sigma_{x_2}}\right) \quad (9)$$

Where σ_{x_1} and σ_{x_2} are the standard deviation of the first and the second dataset abundances respectively.

We use this standard methodology because the quantity of data is large in all cases, and then the data distribution behaves as a normal distribution, resulting in a robust correlation coefficient (Lanzante, 1996).

3.2. Other comparisons as a function of space and time

Here we compare the climatologies of H_2O, HDO~~,~~ and ~~the isotopic ratio between HDO and H_2O, typically noted by~~ δD. In this approach, each grid box represents an average over several measurements. It has the advantage of not requiring coincidences. Therefore, the databases are larger, but the weakness is that sampling biases can affect the comparison.

We first performed the data binning. x_i ($\sout{I,}\bar{\theta}, \sout{\bar{\phi},} t, z$) is the individual concentration of ~~the isotopologue I (~~H_2O~~, or~~ HDO or δD~~)~~ for a given time t, a latitude $\bar{\theta}$~~, a longitude $\bar{\phi}$~~ and for an altitude z. We average the data sets that match the condition for belonging to a given bin.

$$I_{\overline{VMR}}(\sout{I,}\bar{\theta},\sout{\bar{\phi},}t,z) = \frac{1}{n_o}\sum_{i=1}^{n_o} x_i(\sout{I,}\bar{\theta},\sout{\bar{\phi},}t,z) \quad (10)$$

where n_o is the amount of data found within the established grid, and $I_{\overline{VMR}}$ is the value representing all the data fulfilling the grid condition (Högberg et al., 2019).

~~Using Eq. (9) and Eq. (10), it is possible to obtain the deuterium excess as:~~

$$\sout{\delta D_{\overline{VMR}}(\delta D,\bar{\theta},\bar{\phi},t,z) = \left[\frac{HDO_{\overline{VMR}}(HDO,\bar{\theta},\bar{\phi},t,z)}{2\cdot VSMOW\cdot H_2O_{\overline{VMR}}(H_2O,\bar{\theta},\bar{\phi},t,z)} - 1\right]\cdot 1000.} \quad \sout{(11)}$$

From the grid box means of H_2O, HDO and δD, several climatologies are compared for the period 2004-2012. The first one is a comparison of latitude - altitude cross sections (zonal means) for a time interval. We analyzed zonal means constructed from 10 deg latitude bins over the seasons December to February and June to August ~~Latitude cross sections comparison is a method for comparing climatologies. The latitude bins were $\Delta\bar{\theta}$=10° and we focused on two different seasons: December-February (DJF) and June-August (JJA).~~ Examining time series is another way to compare the data. The time series used in this section

are based on monthly zonal means obtained considering the latitude range from 30º S to 30º N for each month. This comparison shows how each database captures seasonal and annual cycles ~~and interannual variability~~. ~~The maps and graphics are smoothed via the smooth function in MATLAB R2021a.~~

4. RESULTS AND DISCUSSION

4.1. Vertical profiles comparisons

The ~~dataset global~~ H_2O average ~~of H_2O~~ profiles for ACE-FTS ~~compared to~~, MIPAS-IMK and ~~to~~ MIPAS-ESA~~,~~ computed on all coincident profiles (2004-2012) and all latitudes~~,~~ are shown in Fig~~s~~. 3 (a) ~~and 3(c), respectively~~. The ~~error~~ bars given for the average profiles are the ~~1 σ~~ standard error ~~deviation~~ of the mean (SEM) distribution of measurements at each altitude level. The ~~vertical coincident~~ profiles of H_2O exhibit a slight increase with altitude in the stratosphere (from 15 km up to 50 km, approximately) both for MIPAS-IMK and MIPAS-ESA, which is consistent with the stronger chemical generation of WV through methane oxidation in the upper stratosphere near 50 km (LeTexier et al., 1988). ACE-FTS average ~~Similar coincident~~ profiles are consistent to the two MIPAS profiles ~~obtained for ACE-FTS in the tropical lower stratosphere (~~up to~~below~~ 30 km~~)~~. In fact, ACE-FTS and MIPAS-IMK profiles between ~~the~~ 20 and 30 km ~~levels~~ are ~~almost the same~~very close ~~for ACE-FTS and MIPAS-IMK~~ (Fig. 3(a)). However, above 30 km, ACE-FTS H_2O profiles have a significant deviation from the other two databases, which was also found in the SPARC/WAVAS-II comparisons for earlier data versions with respect to many other satellite data records (see e.g., Lossow et al., 2019)~~The higher values of MIPAS-IMK in the tropopause region are due to the limited vertical resolution in these levels as indicated in previous works (e.g., Hegglin et al., 2013) (Fig. 3(a)). In ACE-FTS, the decrease of the mean WV concentration with altitude is less pronounced in the upper stratosphere and the lower mesosphere (Figs. 3(a) and 3(c)). However, the dispersion of the data around the measure of mean indicates that the data between 12 to 30 km are comparable in the three databas Högberg et al. (2019) compares the global average H_2O vertical profiles from previous version of ACE-FTS and MIPAS-IMK (MIPAS-IMK v5 and v20, and ACE-FTS V3.5) for the MIPAS high-resolution period (2002-2004). The obtained results exhibit a high degree of similarity to the findings reported in previous studies (Högberg et al., 2019).~~ Coincident H_2O profile comparisons between ACE-FTS and MIPAS (IMK and ESA) reveal the presence of a minimum ~~for both H_2O and HDO~~ around the tropopause at 17 km of altitude. ~~Specifically, ACE-FTS demonstrates a global minimum for H_2O at 15 km, with a concentration of 4.02 ± 0.72 ppmv, while MIPAS-IMK exhibits a similar minimum at 15 km, with a concentration of 4.28 ± 0.69 ppmv. In the case of ACE-FTS and MIPAS-ESA, MIPAS-ESA displays a distinct minimum at 13 km, measuring 4.40 ± 1.03 ppmv. Conversely, the global minimum for HDO in the coincident profiles is consistently observed at an altitude of 16 km across all cases. Specifically, ACE-FTS and MIPAS-IMK demonstrate a minimum concentration of 0.54 ± 0.13 ppbv and 0.56 ± 0.25 ppbv, respectively, while the coincident profiles of ACE-FTS and MIPAS-ESA yield a minimum of 0.53 ± 0.13 ppbv for ACE-FTS and 0.58 ± 0.24 ppbv for MIPAS-ESA.~~

The ~~dataset~~ average ~~Global mean of~~ HDO vertical profiles ~~of HDO~~, along with the~~ir~~ standard error of the means ~~deviations~~ are shown for the three databases~~ACE-FTS and MIPAS-IMK~~ in Fig. 3(b) ~~and for ACE-FTS and MIPAS-ESA in Fig. 3(d)~~. ACE-FTS and MIPAS-IMK~~The~~ ~~global~~ average ~~results~~ profiles are almost identical ~~when comparing ACE-FTS and MIPAS-IMK~~ in the range between 1~~2~~5 ~~to~~ and 48~~50~~ km ~~(Fig. 3(b))~~. ~~However, On a global average, when the~~ MIPAS-ESA dataset ~~is compared with the two above mentioned databases it~~ is ~~also~~ almost identical ~~compared to ACE-FTS~~ to the other two datasets in the lower stratosphere (1~~3~~0 to 3~~4~~0 km) ~~and~~but~~but~~ exhibits a dry bias ~~compared to ACE-FTS~~ in the upper stratosphere (i.e., above ~~between 20 to~~ 34 ~~50~~km, see Fig. 3(~~b~~d)), ~~,although according to the uncertainties, this dry bias is not significant~~. ~~The global minimum value around the tropopause for HDO coincident profiles is consistently observed at an altitude of 16 km across all databases. Specifically,~~ ACE-FTS and MIPAS-IMK demonstrate a minimum concentration at 16 km of altitude~~of 0.54 ± 0.13 ppbv and 0.56 ± 0.25 ppbv, respectively~~, while the coincident profiles of ACE-FTS and MIPAS-ESA yield a minimum ~~of 0.53 ± 0.13 ppbv~~around the 12km region~~for ACE-FTS and 0.58 ± 0.24 ppbv for MIPAS-ESA~~. Högberg et al. (2019) also compared HDO profiles ~~from~~ to ~~the above mentioned~~ previous versions of the MIPAS-IMK and ACE-FTS for the period February – March 2004. They demonstrated a high consistency in the structures along the stratosphere between the two databases. They showed a dry bias of MIPAS-IMK in the tropopause ~~and the lower mesosphere of roughly 0.1 ppmv~~, which does not exist ~~. i~~In this new version of the data~~. , the dry bias is present in comparison to ACE-FTS, but it is even more reduced.~~

The average δD vertical profiles of the three databases are in reasonable agreement from 13 to 30 km of altitude (Fig 3 (c)). Above 30 km ACE-FTS δD mean profile shows a positive bias compared to the two MIPAS databases, probably derived from the dry bias of ACE-FTS H_2O data. On the other hand, MIPAS-ESA δD depicts a negative bias from 33 km upwards, probably derived from the MIPAS-ESA HDO dry bias at these altitudes. The optimal level of agreement between the three data sets is observed in the altitude range between 16 and 30 km, to which we will restrict the climatological comparisons.

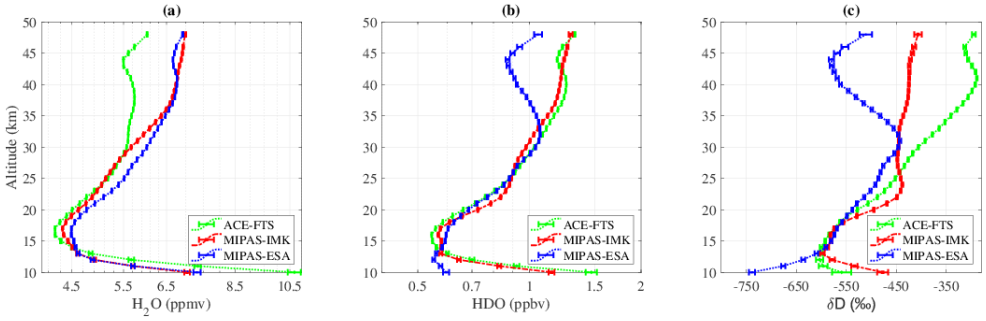

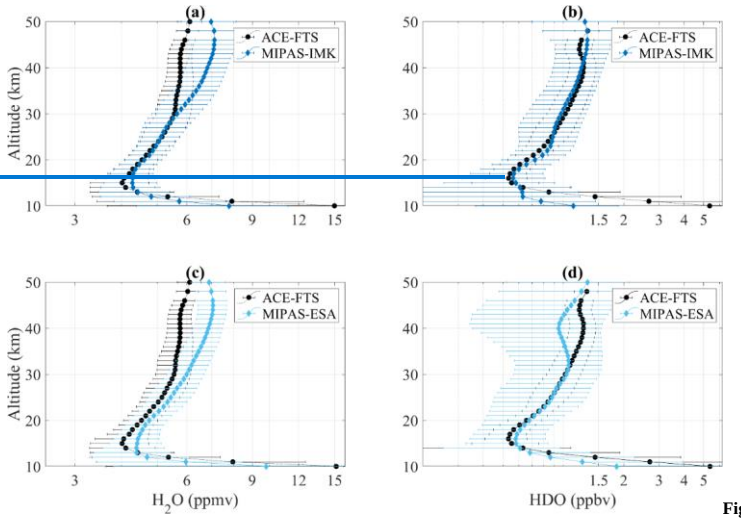

Figure 3. ~~Global~~ A~~a~~veraged vertical profiles comparison between ACE-FTS (green diamonds~~black dots~~), ~~and~~ MIPAS-IMK (red squares~~blue dots~~) and MIPAS-ESA (blue asterisks)~~are shown~~ for (a) H_2O observations, ~~and~~ (b) HDO observations and (c) δD. ~~Global averaged vertical profiles comparison between ACE-FTS (black dots) and MIPAS-ESA (blue dots) are shown for (c) H_2O observations and (d) HDO observations.~~ The ~~error~~ bars represent the ~~1σ~~ standard error of the mean~~deviation~~.

4.2. Bias comparison

Figure 4 shows the biases derived from the profile-to-profile comparisons as described in section 3.1.1~~3~~. As shown above, the comparisons are typically based on several thousand coincidences above approximately 15 km, and cover latitudes from 90° S to 90° N for the 2004-2012 period.

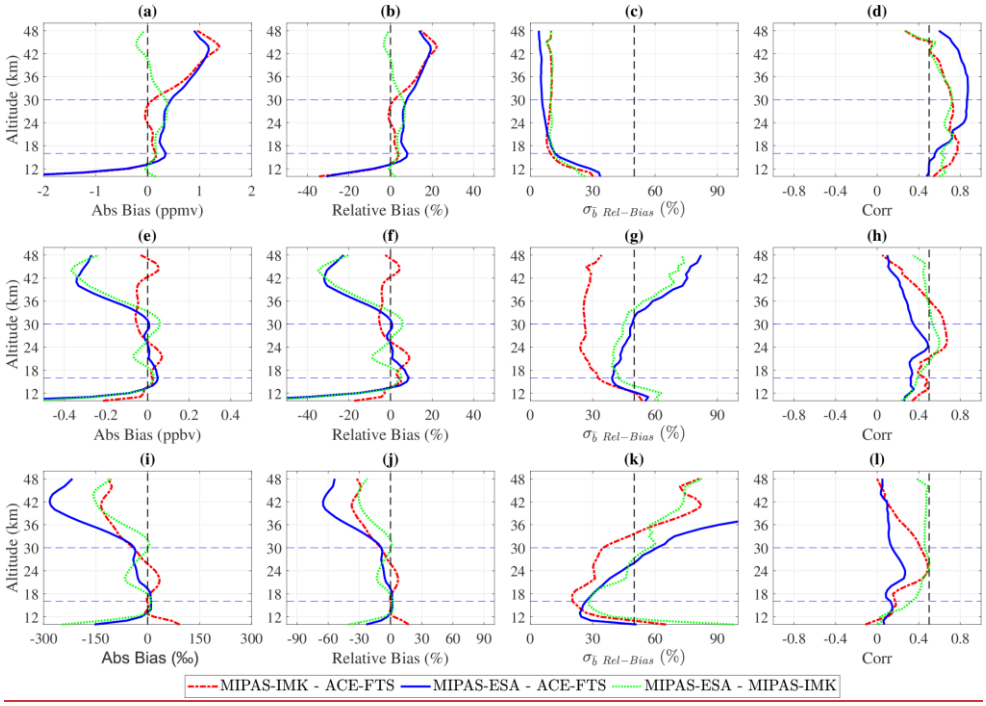
(a)
(b)
(c)
(d)
(e)
(f)
(g)
(h)
(i)
(j)
(k)
(l)
Altitude (km)
Abs Bias (ppmv)
Relative Bias (%)
$\sigma_{\bar{b}\ Rel-Bias}$ (%)
Corr
Abs Bias (ppbv)
Abs Bias (‰)
MIPAS-IMK - ACE-FTS
MIPAS-ESA - ACE-FTS
MIPAS-ESA - MIPAS-IMK

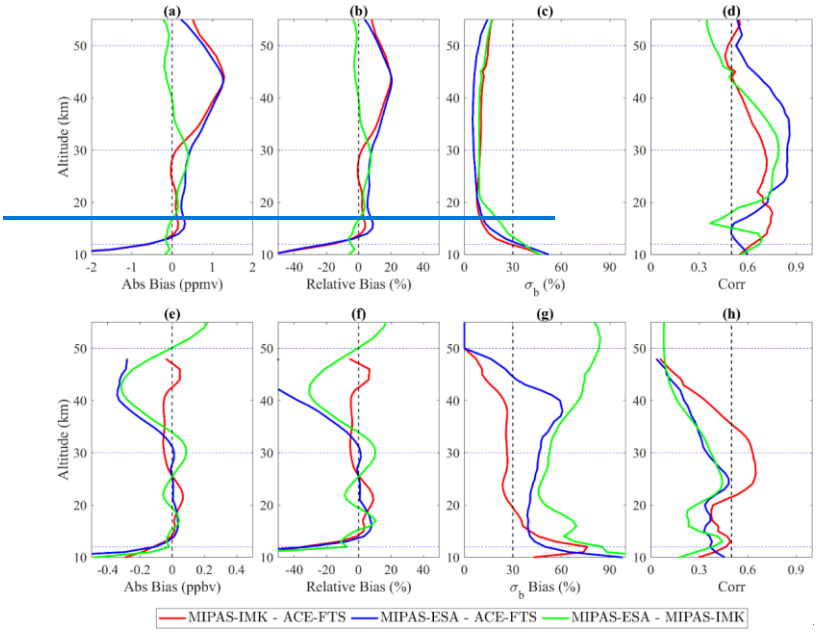

Figure 4. Comparisons between MIPAS-IMK, MIPAS-ESA and ACE-FTS for H_2O (top panels), ~~and~~ HDO (middle~~bottom~~ panels) and δD (bottom panels): (a, e, i) the absolute bias, (b, f, j) the relative bias, (c, g, k) the de-biased standard deviation of the relative bias and (d, h, l) correlation. Black dashed lines indicate 0 ppbv, 0%, 5~~3~~0% and 0.5 from left to right in the different panels. Blue dashed lines indicate the 16 km and the 30 km levels. Maximum and minimum values obtained for the range 16−30 km are indicated in Table 1.

For H_2O, t~~T~~here is a good agreement between the three datasets in ~~the H_2O absolute bias~~ an altitude range between 16 km and 30 km ~~for the three databases~~ (Fig. 4(a)), with biases close to zero between MIPAS-IMK and ACE-FTS. Between MIPAS (IMK and ESA) and ACE-FTS, the absolute bias reaches values greater than 1 ppmv near the 40 km region. The relative biases observed in the three analyzed cases for the lower and middle stratosphere (16~~0~~ – ~~3~~0 km) are all below ~~8.9~~ ~~1~~8.2%, as depicted in Fig. 4(b). ~~The comparisons of the MIPAS-IMK data set with the coincident MIPAS-ESA profiles show relative biases less than 7.6 % in the middle stratosphere (close to 30 km). The relative biases observed in the three analyzed cases for the lower stratosphere (10-30 km) are all below 8.9 %, as depicted in Fig. 4(b).~~ Beyond the altitude of 30 km, the relative biases increase with altitude in the comparisons with the MIPAS-ESA~~ACE-FTS~~ data set exhibiting values exceeding 209.0 %, ~~increasing with altitude until reaching~~around approximately the 40 km region, where the bias starts to decrease. Figure 4 (c) shows the comparison between the ~~H_2O~~ de-biased standard deviations of H_2O obtained by comparing the data sets. All the results show

a good agreement and small variations in all the stratosphere. It is worth mentioning that lower de-biased standard deviations are found in the MIPAS-ESA to ACE-FTS comparison above 25 km of altitude coupled with the higher correlations of these datasets (Fig 4(d)), which is consistent with the MIPAS-IMK retrievals being less sensitive to actual atmospheric variations in H_2O. ~~Lower correlation coefficients (0.37) are observed in the 15 km to 18 km altitude range in the MIPAS-IMK and MIPAS-ESA comparisons, related to higher standard deviation values (22.6 %).~~

HDO absolute differences between the three datasets~~bias~~ are within ± 0.1 ppbv ~~varies from -0.56 to 0.07 ppbv~~ in the 16 to 30 km altitude range (Fig. 4(e)). The HDO relative biases reach values up to ~~for HDO ranges from -8.7 2 to~~ 9.12 ~~-~~% (Fig. 4(f)) between the same altitudes. The HDO de-biased standard deviations (Fig. 4(g)) show~~s~~ values lower than ~~of~~ 50 ~~-~~%. Conversely to H_2O, the lower de-biased standard deviations for HDO are found for the MIPAS-IMK to ACE-FTS comparison above the 15 km region, which is coupled with its higher correlation coefficients and consistent with the MIPAS-ESA retrieval being less sensitive to atmospheric variations of HDO.~~The lowest correlation coefficients (below of 0.44) are also found for MIPAS-ESA comparisons (Fig. 4(h)), with a minimum correlation of 0.23 and 1-σ of 69.4 % in the range between 15 and 18 km.~~

The comparison of δD (see Fig. 4 (i) for absolute differences and Fig. 4 (j) for percent differences) shows an agreement within 8.5 % between ACE-FTS and MIPAS-ESA and within 13.4% for MIPAS-ESA and MIPAS-IMK in the range between 16 km and 30 km approximately. Larger biases are found above 30 km where the largest deviations are found in the MIPAS-ESA and ACE-FTS comparisons, due to ACE-FTS negative bias in H_2O and MIPAS-ESA negative bias in HDO. The smaller relative de-biased standard deviation in the lower and the middle stratosphere (Fig. 4 (k)) is found for ACE-FTS and MIPAS-IMK comparison (between 20 and 34%), consistent with the larger random noise of MIPAS-ESA HDO. Pearson correlation coefficients are greater than 0.4 with the comparisons between MIPAS-ESA and MIPAS-IMK datasets (Fig. 4 (l)). The correlation coefficients in the δD comparisons of the ACE-FTS and MIPAS-ESA data show the lowest agreement with values in the range of 0.1 and 0.2 for the lower and middle stratosphere.

These results are i~~I~~n accordance with ~~previous~~ comparisons by Högberg et al. (2019) between MIPAS-IMK and ACE-FTS ~~datasets~~with previous versions of the data for a very limited overlap period (from February 2004 to March 2004), where relative biases for H_2O, HDO and δD were found to be smaller than 10~~.0~~ % in the middle stratosphere. However, in our current study, δD deviations in the UTLS region show lower values than the biases founded by these authors. ~~For HDO, the relative biases remain below 10.0 %, which is consistent with the findings of Högberg et al. (2019). Moreover, the comparison reveals similar behaviour below 12 km and above 35 km, where the relative biases exceed the 10.0 % threshold.~~ For MIPAS-ESA, Raspollini et al. (2020) also showed the HDO mean absolute and relative bias between MIPAS-ESA and ACE-FTS V~~v~~4.1/4.2 data.

However, they use different coincidence criteria for the determination of coincident profiles, and thusen, their results are not directly comparable.

In order to understand the differences between the two MIPAS databases and the fact that, in some cases, the two MIPAS datasets are more different than MIPAS and ACE-FTS we have to consider that there are differences in the algorithms, in the selected spectral points, but also in the used spectroscopic database (MIPAS-ESA using spectroscopic data for H_2O and HDO based on HITRAN 2012, while MIPAS-IMK using data based on HITRAN 2008) and in the used radiances (MIPAS-ESA using the last release of L1V8 data, while MIPAS-IMK using L1V5 data). L1V8 data have been corrected with an upgraded radiometric calibration (Kleinert et al., 2018), impacting both the radiance and its temporal drift.

Discrepancies in the troposphere and upper levels of the stratosphere derived from the bias analysis indicate that the three databases are comparable only between 16 to 30 km. Therefore, in the following, the climatological analysis will be restricted to the range of the lower and the middle stratosphere. Tables 1 and 2 summarises the datasetglobal average characteristics of the H_2O, and HDO and δD comparisons between 16 to 30 km for the period 2004-2012. The results come from coincident profiles for the full globe without latitude restriction.

Table 1. H_2O, HDO and δD range of the statistical quantities for the comparison of the databases between 16 to 30 km of altitude for the full globe as summary of Fig. 4. Absolute bias (Abs. bias), relative bias (Rel. bias), De-biased standard deviation (De-biased SD) and Pearson correlation coefficient (r) values are indicated.

		MIPAS-IMK – ACE-FTS	MIPAS-ESA – ACE-FTS	MIPAS-ESA – MIPAS-IMK
Abs. Bias	H_2O (ppmv)	−0.05 to 0.16	0.23 to 0.45	0.15 to 0.38
	HDO (ppbv)	−0.05 to 0.07	−0.02 to 0.05	−0.07 to 0.06
	δD (‰)	−40.75 to 34.96	−41.22 to 10.45	−65.59 to 11.28
Rel. Bias (%)	H_2O	−0.9 to 3.7	5.1 to 8.2	3.2 to 6.8
	HDO	−5.1 to 9.1	−1.8 to 8.7	−8.7 to 5.9
	δD	−9.4 to 7.3	−8.5 to 1.8	−13.4 to 2.0
De-biased SD (%)	H_2O	7.9 to 9.9	5.6 to 11.8	9.2 to 11.4
	HDO	24.0 to 32.5	39.3 to 49.0	39.2 to 44.6
	δD	20.1 to 34.0	26.7 to 60.9	28.0 to 57.4
r	H_2O	0.7 to 0.8	0.6 to 0.9	0.6 to 0.7
	HDO	0.4 to 0.7	0.3 to 0.5	0.4 to 0.6
	δD	0.2 to 0.5	0.1 to 0.3	0.3 to 0.5

~~**Table 1. H_2O range of the statistical quantities for the comparison of the databases between 16 to 30 km of altitude for the full globe. From left to right: the mean absolute bias, the mean relative bias, the debiased standard deviation and the correlation coefficient.**~~

	~~Bias Abs.~~	~~Bias Rel.~~	~~1σ Bias~~	~~Corr.~~

Con formato: Fuente: (Predeterminada) +Cuerpo (Times New Roman)

	~~H_2O (ppmv)~~	~~H_2O (%)~~	~~H_2O (%)~~	
~~MIPAS-IMK vs ACE-FTS~~	~~-0.03 _ 0.15~~	~~-0.7 _ 4.0~~	~~7.7 _ 11.1~~	~~0.69 _ 0.75~~
~~MIPAS-ESA vs ACE-FTS~~	~~0.22 _ 0.45~~	~~5.4 _ 8.9~~	~~5.8 _ 13.0~~	~~0.51 _ 0.85~~
~~MIPAS-ESA vs MIPAS-IMK~~	~~-0.06 _ 0.40~~	~~-1.7 _ 7.6~~	~~9.1 _ 22.6~~	~~0.37 _ 0.79~~

~~**Table 2. HDO range of the statistical quantities for the comparison of the databases between 16 to 30 km of altitude for the full globe. From left to right: the mean absolute bias, the mean relative bias, the debiased standard deviation and the correlation coefficient.**~~

	~~Bias Abs. HDO (ppbv)~~	~~Bias Rel. HDO (%)~~	~~1σ Bias HDO (%)~~	~~Corr.~~
~~MIPAS-IMK vs ACE-FTS~~	~~-0.05 _ 0.07~~	~~-4.9 _ 9.2~~	~~23.7 _ 36.2~~	~~0.37 _ 0.65~~
~~MIPAS-ESA vs ACE-FTS~~	~~-0.01 _ 0.04~~	~~-1.0 _ 8.1~~	~~39.0 _ 46.4~~	~~0.33 _ 0.48~~
~~MIPAS-ESA vs MIPAS-IMK~~	~~-0.06 _ 0.09~~	~~-8.7 _ 10.6~~	~~45.9 _ 69.4~~	~~0.22 _ 0.44~~

H_2O biases in the lower and middle stratosphere (16 km to 30 km) ranged from -0.05ppmv to 0.45 ppmv across the three databases. Lower H_2O absolute and relative biases are found for the MIPAS-IMK–ACE-FTS comparison with values up to 0.16 ppmv and 3.7% respectively. Lower de-biased standard deviations (up to 9.9%) and higher correlation coefficients (from 0.7 to 08) are found in the same databases comparison. Therefore, H_2O profiles from MIPAS-IMK and ACE-FTS are in better agreement than compared to MIPAS-ESA dataset. For HDO, lower absolute and relative biases are found in the MIPAS-ESA–ACE-FTS comparisons with values up to 0.05 ppbv and 8.7% respectively. The lower δD values for both absolute and relative biases are found for the same comparison as HDO (MIPAS-ESA–ACE-FTS) up to 41.2‰ and 8.5% respectively. However, the de-biased standard deviations reach values of 49% and 61% for HDO and δD respectively. Only the comparison between the correlation coefficients for δD obtains the better result for the two MIPAS datasets with values from 0.3 to 0.5.

~~The relative biases in the lower stratosphere show a difference of less than 8.9 % but higher than -0.7 % for H_2O (Table 1) as shown in the Fig. 4. The comparison between MIPAS-IMK and ACE-FTS has a 1-σ standard deviation within the range of 7.7 to 11.1 %, and a maximum correlation of 0.75. On the other hand, The average difference between MIPAS-ESA and ACE-FTS in the lower stratosphere is ranging 5.4 to 8.9 %, exhibiting a wet bias and well within the 1-σ standard deviation of 5.8 to 3.0 % and has a maximu correlation coefficient of 0.85. Finally, quantifying the H_2O differences between MIPAS-ESA and MIPAS-IMK in the lower levels of the stratosphere, a dry bias of 1.7 % was observed at an altitude of 16 km. Within lower stratosphere region, the relative bias exhibited a range of - 1.7 to 7.6 %, well within the 1-σ standard deviation . of 22.6 % in the range of 9.1 to 22.6 % and a correlation coefficient of 0.37 at 16 km. The correlations in the lower levels of the stratosphere were between 0.37 to 0.79.~~

Con formato: Fuente: (Predeterminada) +Cuerpo (Times New Roman)

Con formato: Fuente: (Predeterminada) +Cuerpo (Times New Roman)

Con formato: Fuente: (Predeterminada) +Cuerpo (Times New Roman)

Con formato: Fuente: (Predeterminada) +Cuerpo (Times New Roman)

Con formato: Fuente: (Predeterminada) +Cuerpo (Times New Roman)

Con formato: Fuente: (Predeterminada) +Cuerpo (Times New Roman)

Con formato: Fuente: (Predeterminada) +Cuerpo (Times New Roman)

~~For HDO (Table 2) the mean absolute bias is much smaller for the three databases in the lower stratosphere and the relative bias is between - 8.7 to 10.6%. In contrast to H_2O, the debiased standard deviation ranges are far larger with values between 23.7 and 69.4 %, and the correlation coefficients are lower, between 0.22 to 0.65.~~

4.3. Comparisons of seasonally averaged latitude cross-sections

Figure 5 shows the seasonally averaged latitude-altitude~~pressure~~ cross sections of H_2O, ~~and~~ HDO and δD for the three data sets considered in the comparisons from 890º S to 890º N. Water vapour shows a large depletion in the tropopause in the three datasets both in JJA (Fig. 5(a)) and DJF (Fig. 5(b)), with values between 3 and 5 ppmv in the lower stratosphere. The depletion in the tropics occurs at a higher altitude than in the mid-latitudes. A secondary minimum in the tropical middle stratosphere is also appreciated in both seasons, associated with the minimum originating in the lower stratosphere during the previous year and propagated upward by the Brewer-Dobson circulation. ~~ACE-FTS might even show a third minimum, at least for DJF.~~ This ascent ~~rate~~ of water vapour in the tropical lower stratosphere by the upwelling branch of the Brewer-Dobson circulation imprints a seasonal cycle of H_2O known as the atmospheric tape recorder (Mote et al., 1996) as will be seen in the next section. With increasing altitude, an increase in H_2O is found to be consistent with the averaged~~global mean~~ vertical profiles shown in Fig. 3. Higher values of H_2O are found first over high latitudes in the summer hemisphere reflecting the production of WV through methane oxidation under a long duration of sunlight (LeTexier et al., 1988). In general, H_2O shows ~~in~~ the zonal mean ~~the~~ expected distribution that has been established in previous studies (e.g., Randel et al., 2001).

The general distribution of HDO (Fig.~~s~~ 5c~~l~~) and 5(d)) shows some similarities to that of H_2O (Fig. 5(a) and 5(b)), reflecting that both species have a common in situ source in the stratosphere, i.e., oxidation of methane and hydrogen~~CH_4 and H_2~~. In Antarctica, both H_2O and HDO values in the polar vortex are lower than for the corresponding Artic polar vortex. These lower values evidence the effect of dehydration through the formation of Polar Stratospheric Clouds (PSCs). However, it is worth commenting that for the ACE-FTS data, the minimum values in the Antarctic polar vortex during the JJA are very low (< 3 ppmv for H_2O and < 0.3 ppbv for HDO) compared to the two MIPAS datasets (in the range of 3.4 to 3.8 ppmv for H_2O and 0.3 to 0.5 for HDO ppbv). ACE-FTS does not include data from all the local winter months because of the requirement for sunlight for its measurements. This requirement leads to ACE-FTS values sampling only during the later part of this season (i.e., August vs. June – August) at the highest latitudes, while the two MIPAS data sample during the three months, and this likely leads to ACE-FTS showing more dehydration than MIPAS.

~~the H_2O and HDO values in the polar winter vortex is less than 2.9 ppmv and 0.33 ppbv, respectively. These low values evidence the effect of dehydration through the formation of~~PSCs,~~Tlikely~~ Fig 5e and 5f depict the δD averaged latitude-altitude cross sections for JJA and DJF respectively. Large differences between the three datasets are found in the tropical upper troposphere due to the influence of clouds and limitations of MIPAS measurements in lower altitudes. Large depletion in δD

is found on top of the climatological tropopause for MIPAS-ESA and ACE-FTS. The depletion occurs in MIPAS-IMK at a higher altitude, especially above the tropical tropopause. It is known that ~~the oxidation of methane in the stratosphere should cause an increase in the isotopic ratio, as~~ water vapour transported from the troposphere to the stratosphere is stronger depleted in the heavier isotopologues while the oxidation of methane in the stratosphere should cause an increase in the isotopic ratio (Wang et al. 2018). The most evident feature at higher altitudes (between roughly 20 and 30 km) is the δD annual cycle with higher values during local summertime and lower values during local wintertime over the high latitudes due to the downwelling of older air which has had more time for methane oxidation (Stiller et al., 2012). This effect is found for the three databases, but there are also differences between them at higher latitudes. In the Antarctic region, the expected asymmetry with latitude driven by the winter polar vortex due to the influence of PSCs on δD values during the austral winter is observed in ACE-FTS data, but it is absent for MIPAS-IMK data. In the case of MIPAS-ESA, the influence of phase transitions related to formation/removal of ice particles on δD in the Antarctic region is very subtle for JJA compared with boreal DJF.

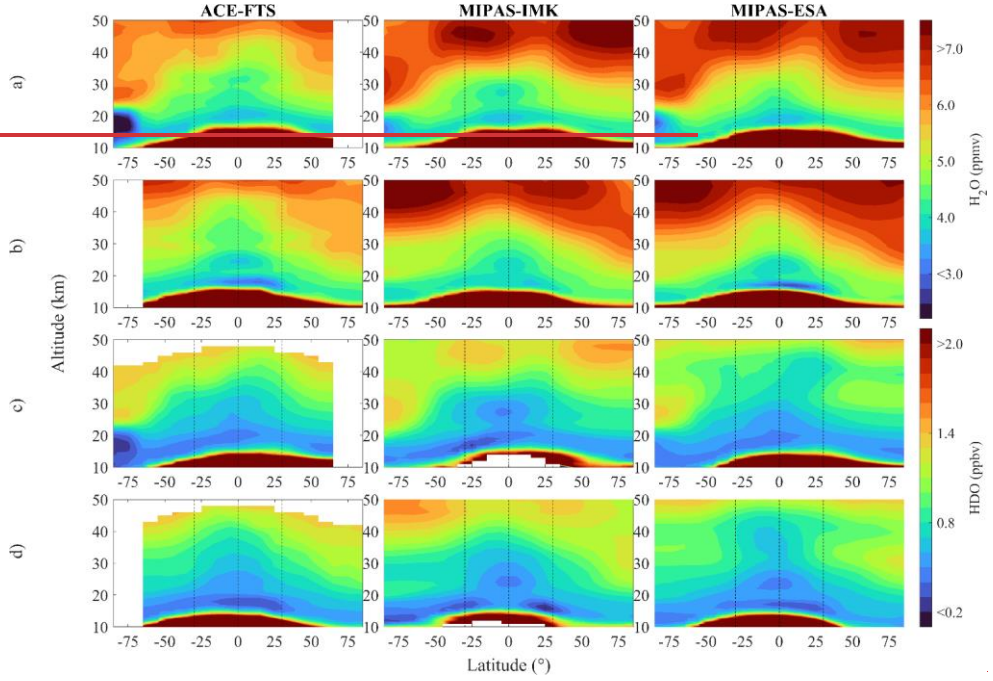

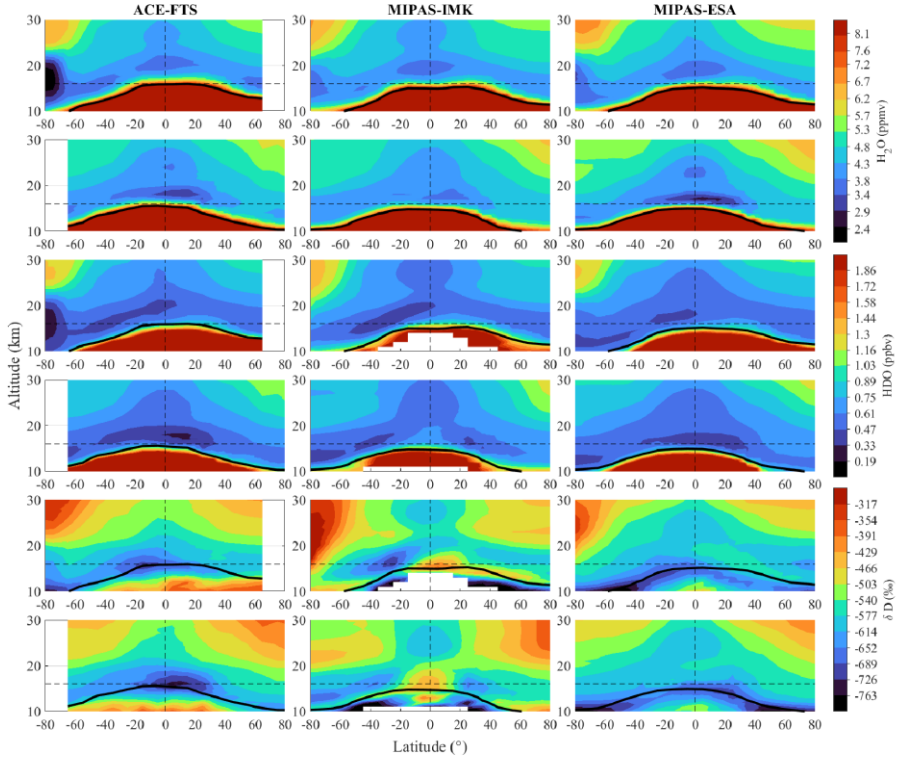

Figure 5. ~~Meridional~~Latitude-altitude cross -sections of H_2O in (a) boreal summer (JJA) and (b) boreal winter (DJF), ~~of~~ HDO for (c) boreal summer and (d) boreal winter ~~for three datasets~~ and δD during I boreal summer and (f) boreal winter for the three datasets. The left column represents ACE-FTS data, the middle column represents the MIPAS-IMK data and the right column the MIPAS-ESA data. The climatology is based on the 2004-2012 period. The absence of profiles in MIPAS- IMK map below the tropical tropopause is due to a more stringent cloud filtering approach used by IMK. Black line indicates the climatological tropopause.

~~The changes in δD mirror changes in H_2O and HDO in the stratosphere (Fig. 6). Above the climatological tropopause, a large depletion in δD is found in the three datasets. During the boreal summer, the latitudinal gradient in δD due to atmospheric dynamics associated with the polar vortex can be distinguished (Fig. 6(a)). However, there is still a relative minimum in δD~~

~~near the tropopause in all latitudes. A secondary minimum about 30 km in the tropical stratosphere is more clearly observed in MIPAS-IMK data and MIPAS-ESA data than in ACE-FTS data, both for summer (Fig. 6(a)) and winter (Fig. 6(b)). Finally, in MIPAS-ESA data, the air above 30 km is not enriched in deuterium as in the other two databases. It is known that the oxidation of methane in the stratosphere should cause an increase in the isotopic ratio, as water vapour transported from the troposphere to the stratosphere is stronger depleted in the heavier isotopologues (Wang et al. 2018).~~ The results obtained with δD for ACE-FTS are in complete agreement with those of Randel et al. (2012) ~~results~~ from previous data versions (2004 to 2009). δD for MIPAS-IMK is only partially in agreement with Högberg et al. (2019) since~~,~~ these authors ~~also~~ observed ~~two~~ minimum values ~~a~~ in the lower stratosphere over the Antarctic polar vortex (75 S to 80 S) during the austral winter in previous version of the data (2002 to 2004)~~, but the minima in Högberg et al. (2019) are less intense than the result in Fig. 6 at 25° S~~. As stated earlier in this work, zonal mean distributions of δD for MIPAS-ESA have never been compared before.

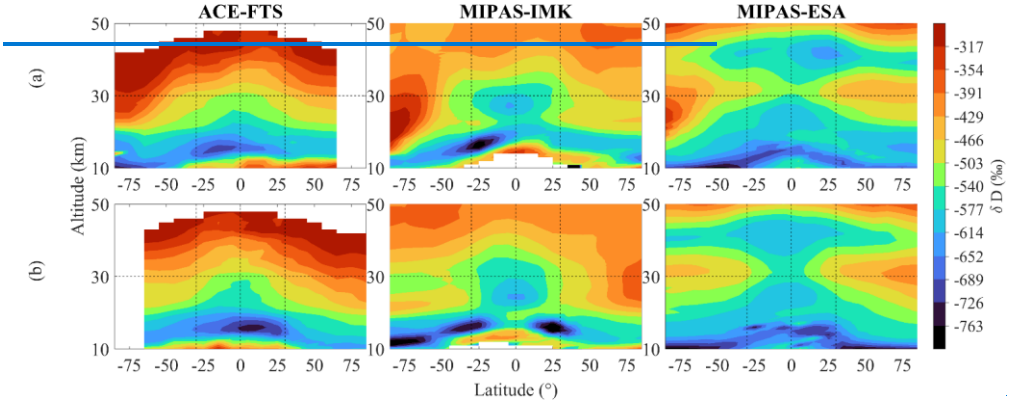

~~**Figure 6. Meridional cross-sections of δD in (a) summer (JJA) and (b) winter (DJF) for the three datasets. The left column represented ACE-FTS data, the middle column the MIPAS-IMK data and the right column the MIPAS-ESA data. The climatology is based on the 2004-2012 period. Data gaps are indicated by white areas; in MIPAS-IMK they are related to the strict cloud-clearing algorithm used to retrieve data.**~~

4.4. Comparison of the tropical seasonal cycle

Several details of the vertical propagation of the tropical seasonal signal along the monthly evolution ~~and the interannual variability~~ of the three databases are shown in Fig. 6~~7~~, which depicts the height-time diagrams covering ~~over~~ 30º S and 30º N of H_2O (left panels)~~, and~~ HDO (central~~right~~ panels) and δD (right panels) concentrations. The graphics are smoothed via the smooth function in MATLAB R2021a. Left panels~~Figures 6(a), 6(b) and 6(c)~~ show~~s~~ minimum annual values in H_2O ~~and HDO~~ originating near the tropical tropopause and propagating vertically upwards, ~~to above 25 km,~~ which is known as the tape recorder signature (Mote et al., 1996). The overall picture is equivalent for the three data sets, but differences in details are

found. ACE-FTS signal is noisier as this dataset has coverage over the tropics typically only for four months (February, April, August, and October). The tape recorder signature is clearly seen but up to 25 km of altitude. The two MIPAS data sets exhibit a stronger tape recorder in terms of its amplitude than the ACE-FTS data. However, for MIPAS-ESA the signal is also larger below 25 km and for MIPAS-IMK the annual variation is found to extend to larger altitudes.

The picture of HDO temporal evolution (central panels) is very similar to the H_2O picture. The exception is that the HDO annual variation in ACE-FTS is found to be weaker and confined to lower levels compared to H_2O annual variation and, by contrast, the tape recorder signature in MIPAS-ESA is extended up to approximately 28 km of altitude and MIPAS-IMK even higher. ~~The interannual variability in ACE-FTS data ((Fig. 7(a)) and MIPAS-IMK ((Fig. 7(b)) data are more similar between them to the MIPAS-ESA interannual variability ((Fig. 7(c)).~~

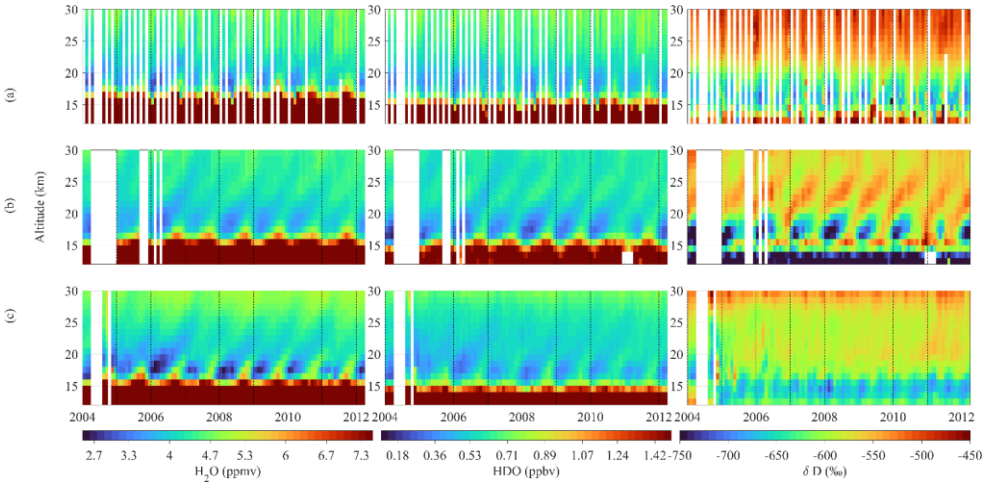

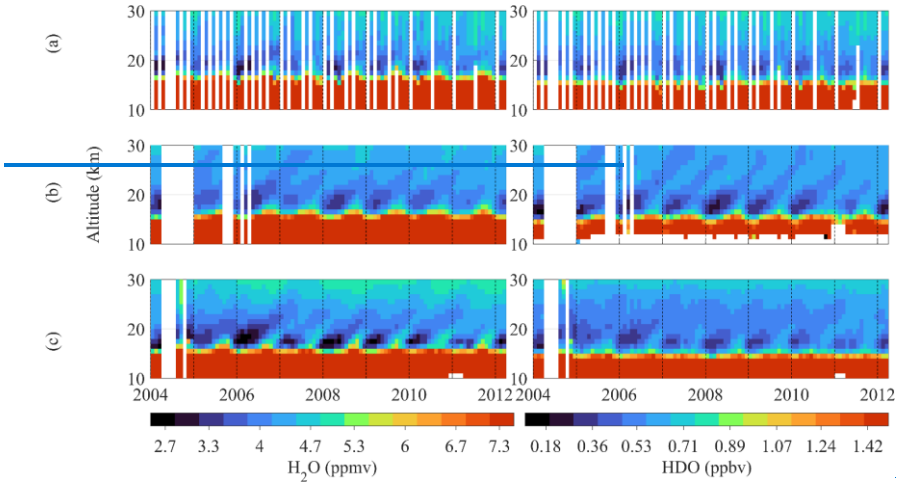

Figure 6~~7~~. Altitude vs. time diagrams over 30º S and 30º N of H_2O, ~~and~~ HDO and δD ~~VMR~~ for the datasets (a) ACE-FTS, (b) MIPAS-IMK, and (c) MIPAS-ESA. ~~White color indicates data gaps.~~ Data coverage between MIPAS-ESA and -IMK differs because IMK data are from the nominal observation mode only, which was not operated in Aug 2004, Sep to Nov 2005, and Feb and Apr 2006, while MIPAS-ESA data cover other observation modes as well.

Right panels depict~~The~~ altitude-time variation~~bility~~ of δD ~~is depicted in Fig. 8~~. Near ~~to~~ 15 km, above the tropopause, a deuterium depletion over the year (compared to SMOW) of roughly -600 ‰ is observed for MIPAS-ESA, -660 ‰ for ACE-FTS and -700‰ for MIPAS-IMK. ACE-FTS data ~~(Fig. 8(a))~~ show ~~small though it shows~~ the characteristic tape recorder pattern of the annual δD minimum, although the annual fluctuations in the lower stratosphere are small. MIPAS-ESA show a very weak signature of the tape recorder which seems to be consistent with ACE-FTS result. By contrast, in MIPAS-IMK, the δD annual variation related to the tape recorder signature is evident ~~(Fig. 8(b))~~ with a steep gradient between the dry and wet phases in the lower stratosphere. Lossow et al. (2020) showed that a tape recorder signal exists in ACE-FTS V~~version~~ 3.5 data as well, although with a lower seasonal amplitude of ~ 25 ‰ in contrast to MIPAS-IMK δD data, that have (in the data version investigated there) a seasonal amplitude of about 75 ‰. Figure 6 demonstrates that the differences in seasonal amplitudes found for older data versions remain for the most recent data versions. ~~Finally, MIPAS-ESA δD shows a minimum in the lower stratosphere with low vertical propagation. In the troposphere near to 14 km, a deuterium depletion (compared to SMOW) of -560 ‰ is observed for MIPAS-ESA, -420 ‰ for ACE-FTS and -470‰ for MIPAS-IMK. As it was previously shown in the Fig.4, the MIPAS instrument shows a negative bias at the troposphere, while the ACE-FTS instrument can measure with higher sensitivity further down in the atmosphere, reaching the upper middle part of the troposphere. For this reason, it is most likely~~

that the ACE-FTS database shows more realistic values of the δD distribution at these altitudes compared to the other instrument.

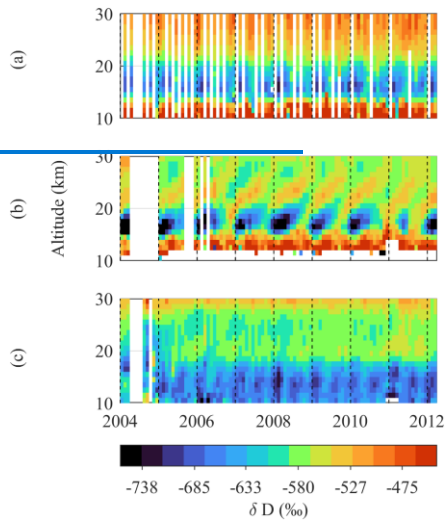

Figure 8. Height-time diagrams of δD in the 30° S-30° N band derived from (a) ACE-FTS observations, (b) MIPAS-IMK observations and (c) MIPAS-ESA observations during 2004-2012.

In Fig. 8, there is a steep vertical gradient in the troposphere for both MIPAS-IMK and ACE-FTS. The dry δD in MIPAS-IMK and ACE-FTS between 14 to 20 km are between -730 to -680 ‰ and -680 to -620 ‰. For MIPAS-ESA I see up to ~18 km mostly blue values around -560 ‰.

SUMMARY AND CONCLUSIONS

The stratospheric water vapor (SWV) has a significant climate feedback, which makes quantitative estimates of SWV budget changes necessary. Furthermore, there still remains many uncertainties related to the origin of the SWV (Konopka et al., 2023) and current climate models show substantial biases in the water vapor content of the lowermost stratosphere (Charlesworth et al., 2023). The entry of water vapor into the stratosphere is controlled by chemical and dynamical processes in the lower stratosphere (LS) presenting a challenge for understanding and modelling this region. By adding the isotopic processes in the analytical and numerical models and by comparing modelled and measured isotopic composition in water vapor, model's transport processes can be directly validated. Therefore, accurate stratospheric δD data is of utmost importance to validate water vapor transport studies and to improve biases in the SWV of climate models.

Previous comparisons of δD data in the stratosphere with MIPAS-IMK and ACE-FTS used a very limited period of time. Högberg et al (2019) assessed the profile-to-profile comparisons of stratospheric δD using the overlap period between the two datasets from February 2004 to March 2004. During this short overlap period most of the coincidences are concentrated near 70 N. Lossow et al. (2020) reassessed the discrepancies in the annual variation of δD in the tropical lower stratosphere, but the MIPAS-IMK dataset only covered the period from July 2002 to March 2004. Therefore, longer time series are needed to draw robust conclusions.

This work presents H_2O, HDO and δD comparisons among 3 data sets of stratospheric and lower mesospheric data from two different satellite instruments, ACE-FTS and MIPAS. The recent data versions ACE-FTS V4.1/4.2, MIPAS-IMK V5H_H2O_20, V5R_H2O_220/221, V5H_HDO_22 and V5R_HD~~2~~O_222/223 and MIPAS-ESA Level 2 V8 were compared. Specifically, the comparison with MIPAS-ESA is performed for the first time in this work for the period 2004 - 2012. The database comparison is based on two approaches: profile-to-profile comparisons, and climatology comparisons not requiring coincidences of the observations. The main conclusions of this study are summarized as follows:

The ~~be~~mean profiles of H_2O, HDO and δD profiles between 16 and 30 km ~~altitude levels~~ averaged over all latitudes, show~~s~~ remarkable similarity between ACE-FTS and MIPAS datasets ~~IMK~~, with only minor differences observed ~~between ACE-FTS and MIPAS-ESA~~ within these altitudes. Above 30 km, the H_2O ACE-FTS data show a dry bias, while MIPAS-ESA data show a dry bias for HDO beyond the same altitude. As consequence, a negative/positive bias was found for MIPAS-ESA/ACE-FTS δD data upwards 30 km of altitude. Therefore, the climatological analysis was restricted to the range between 16 and 30 km which corresponds to the lower and the middle stratosphere. ~~Discrepancies can be observed above 30 km in MIPAS (IMK and ESA) vs ACE-FTS, but according to the uncertainties, they are not significant. The global HDO profiles are almost identical when comparing ACE-FTS and MIPAS-IMK. In the case of MIPAS-ESA, a negative difference is depicted in the upper levels of the stratosphere, but it is within the 1-σ standard deviation of the global average coincident profiles. The analysis conducted in this study highlights a higher level of agreement in HDO measurements obtained from ACE-FTS in both comparison cases. These findings contribute to our understanding of the agreement and discrepancies among the datasets analyzed in this study. The results are quite similar to those obtained by Högberg et al. (2019) for previous versions of MIPAS-IMK and ACE-FTS for the period 2002-2004.~~

Biases from profile-to-profile comparisons exhibited the quantitative differences between the ~~global~~ average profiles. Coincident profiles at all latitudes indicate a general good agreement in ACE-FTS comparisons for H_2O, HDO and δD within ±13.4% in the relative bias for the altitude range 16 – 30 km. For H_2O the better agreement is found between MIPAS-IMK and ACE-FTS with values in the range −0.05 to 0.16 ppmv (−0.9% to 3.6%). However, comparisons between MIPAS-ESA and ACE-FTS show the lower absolute and relative bias both for HDO (−0.02 to 0.05 ppbv and −1.8 to 8.7%) and δD (−41.2

to 10.5‰ and −8.5 to 1.8%). The δD measurements obtained here are comparable to those obtained by Högberg et al. (2019) for previous versions of MIPAS-IMK and ACE-FTS data. Högberg et al. (2019) performed four comparisons between different MIPAS-IMK vs. ACE-FTS versions obtaining biases in δD typically within ±30‰ (corresponding to ±10% in relative terms) for the lower and middle stratosphere. In this work, similar biases are found within the same altitude range. Furthermore, our results are considerably more robust than those of Högberg et al. (2019) because of the limited period of time analysed by these authors (from the second half of February 2004 to end of March 2004), with the number of coincident profiles varying between 300 and 400. Our comparisons are typically based on several thousand coincidences during a time period of 9 years. Furthermore, our results are complemented by the comparisons with new MIPAS-ESA data, which indicate for δD even a better agreement with ACE-FTS than MIPAS-IMK - ACE-FTS agreement.

~~H2O biases in the lower stratosphere (16 km to 30 km) ranged from -1.6 % to 8.9 % across the three databases. The largest biases were found just above 35 km in MIPAS (ESA and IMK) vs ACE-FTS comparisons, reaching maximum deviations of 20.1 % and 20.5 % at 43 km (ESA) and 44 km (IMK) respectively. The 1-σ standard deviation among the databases ranged from 5.7 % to 22.6 %. Correlation coefficients were mostly above 0.5, except for MIPAS-IMK vs MIPAS-ESA comparisons in the upper 500 troposphere and lower mesosphere. The HDO biases observed within 16 km and 30 km exhibit reduced variability and consistently remain below 10.6 %. Specifically, when comparing HDO measurements between ACE-FTS and MIPAS-IMK, a positive bias of less than 10.2 % and a negative bias exceeding -2.9 % are observed. HDO biases agreed with Högberg et al. (2019), ranging from -8.7 % to 10.6 % in MIPAS-IMK vs ACE-FTS. For MIPAS-ESA, Raspollini et al. (2020) used a different method for coincident profile determination, making direct comparisons of HDO biases with our study unfeasible. In terms of 505 combined precision and Pearson correlation coefficient, comparisons involving MIPAS-ESA showed poorer performance compared to MIPAS-IMK and ACE-FTS. Lower correlation and higher 1-σ values were observed in the 14 km to 17 km altitude range, which corresponds to the tropical tropopause region.~~

We also analysed~~overviewed~~ latitude-altitude ~~meridional~~ cross sections ~~in the three databases~~ considering all measurements of the datasets in the latitude range from 80 S to 80 N. Consistent with previous observations (Randel et al., 2012; Högberg et al., 2019), the overall vertical structure of H_2O, ~~and~~ HDO and δD exhibits a large depletion near the tropopause, and higher mixing ratios between 20 and 30 km over the poles during the local summertime ~~and a secondary minimum above in the tropical region and an increase in H_2O and HDO with altitude~~ because of the methane oxidation. However, there are also some differences between the results of each dataset. The tropical depletion of δD in ACE-FTS and MIPAS-ESA occur on the top of the dynamical tropopause, but the minimum is found at higher altitudes in the MIPAS-IMK dataset. Large differences are also found between the two MIPAS data sets over the tropical upper troposphere, probably related to a different approach used by the two MIPAS algorithms to handle cloud contamination. In agreement with Hogberg et al (2019) and because ACE-FTS instrument measures at lower altitudes, it can be concluded that ACE-FTS data are probably more realistic at these altitudes. Regarding the Antarctic region, ACE-FTS shows lower δD values over the polar vortex than the MIPAS datasets, likely related

to PSCs. Nevertheless, the ACE-FTS lower values can be partially attributed to sampling error as ACE-FTS data only cover a 15-days period during the late winter. These results are not representative of the 3-month season mean of MIPAS measurements, which also includes the first months of the winter when the PSCs areal coverage has not yet peaked. MIPAS-ESA barely shows δD minimum values over the Antarctic polar vortex and MIPAS-IMK data do not show them over the highest latitudes. Latitude-altitude sections of δD for MIPAS-ESA have never been shown before.~~An exception here for HDO is the MIPAS-ESA data set which shows the secondary minimum in HDO at higher altitudes than in MIPAS-IMK and ACE-FTS. MIPAS-ESA practically doesn't show the HDO increase at high latitudes and altitudes. The vertical structure of δD is in good agreement with previous versions of MIPAS-IMK and ACE-FTS data (Randel et al., 2012; Högberg et al., 2019). Latitude-altitude sections of δD for MIPAS-ESA have never been shown before and they exhibit distinct discrepancies with the other two databases.~~

Finally, the general depiction of the tape recorder signal in H_2O and HDO for the three databases seems to be reasonable. However, the temporal variations of δD in the lower and middle stratospher~~eic δD~~ show more discrepancies. ~~different signals. MIPAS-ESA depicts minimal variations in δD in the lower stratosphere with some short vertical propagations each year. ACE-FTS shows slight discrepancies with MIPAS-IMK as in the previous versions of the data (Randel et al., 2012).~~ The annual variation for ACE-FTS data and MIPAS-ESA data is very weak compared to the MIPAS-IMK dataset, which shows a coherent tape recorder signal clearly detectable up to at least 30 km. Lossow et al (2020) showed a similar result with previous versions of MIPAS-IMK and ACE-FTS data. They performed some tests to reveal the main reason for the differences in the annual variation of δD. They found that while the differences in the temporal sampling between the MIPAS-IMK and ACE-FTS data sets are not the main reason for the differences in the annual variation of δD at least in the lowermost stratosphere, some issues related to the quality of the MIPAS H_2O data used in this context, and the differences in vertical resolution between H_2O and HDO potentially contributed to the δD tape recorder differences between MIPAS-IMK and ACE-FTS. This issue remains open.

Considering that MIPAS and ACE-FTS are the only instruments so far which have measured or are measuring both H_2O and HDO simultaneously from satellite on a long period, further improvements in the data sets are highly welcome to understand and reduce the differences in the zonal mean distributions and the annual variation of δD. With this knowledge, the representation of stratospheric water vapor in models would be improved offering promising prospects for future research.

Code availability

The~~ scripts for data extraction, profile-to-profile comparison, and climatological analysis~~~~ode~~ in MATLAB is available from the authors upon request.

Data availability

The MIPAS-IMK H_2O and HDO datasets can be accessed from the website of the Institute of Meteorology and Climate Research / Atmospheric Trace Gases and Remote Sensing Division (IMK-ASF) at https://www.imk-asf.kit.edu/english/308.php. ~~For HDO data, information can be obtained upon request.~~ The ACE-FTS data can be accessed and downloaded from the website https://databace.scisat.ca/level2. The MIPAS-ESA data is available online and can be downloaded from the FTP server ftp://mip-ftp-ds.eo.esa.int/ using an FTP client.

Author contribution:

L.A. P.O and G.P.S. conceived and designed the research. K.DLR. developed the analysis. P.O and K.DLR. prepared the manuscript draft. K.DLR., P.O., G.P.S. M.K., P.R., M.G., K.A.W., C.P-O. and L.A. reviewed and edited the manuscript. All authors have read and agreed to the published version of the manuscript.

Competing interests:

One of the authors (G.P.S.) is associate editor of AMT.

Acknowledgements

This research has been supported by the following grants: the Spanish Ministerio de Economía y Competitividad (grant no. CGL2016-78562-P), PAPIIT (DGAPA-UNAM) IN116120, IG101423 and CONACyT 315839. Paulina Ordoñez is grateful for the support of Maria Zambrano (UPO; Ministry of Universities; Recovery, Transformation and Resilience Plan -Funded by the European Union -Next Generation EU). The Atmospheric Chemistry Experiment (ACE) is a Canadian-led mission mainly supported by the CSA and the NSERC, and Peter Bernath is the principal investigator. The IMK team would like to thank the European Space Agency for making the MIPAS level-1b data set available. We acknowledge Michael Kiefer for his assistance with IMK data management and providing comments during the early phase of the manuscript. Karen de los Rios is grateful to the National Council on Science and Technology (CONACYT) for their generous financial support and scholarship. Special appreciation is extended to J. R. Torres-Castillo for his invaluable assistance in enhancing the employed algorithms. Additionally, Karen de los Rios acknowledges R. Stanley Molina-Garza for his insightful recommendations.

References

Bernath, P. F., McElroy, C. T., Abrams, M. C., Boone, C. D., Butler, M., Camy-Peyret, C., Carleer, M., Clerbaux, C., Coheur, P.-F., Colin, R., DeCola, P., DeMazière, M., Drummond, J. R., Dufour, D., Evans, W. F. J., Fast, H., Fussen, D., Gilbert, K., Jennings, D. E., Llewellyn, E. J., Lowe, R. P., Mahieu, E., McConnell, J. C., McHugh, M., McLeod, S. D., Michaud, R., Midwinter, C., Nassar, R., Nichitiu, F., Nowlan, C., Rinsland, C. P., Rochon, Y. J., Rowlands, N., Semeniuk, K., Simon, P., Skelton, R., Sloan, J. J., Soucy, M.-A., Strong, K., Tremblay, P., Turnbull, D., Walker, K. A., Walkty, I., Wardle, D. A., Wehrle, V., Zander, R., and Zou, J.: Atmospheric chemistry experiment (ACE): Mission overview, Geophys. Res. Lett., 32, 1–5, https://doi.org/10.1029/2005GL022386, 2005.

Boone, C. D., Nassar, R., Walker, K. A., Rochon, Y., McLeod, S. D., Rinsland, C. P., and Bernath, P. F.: Retrievals for the atmospheric chemistry experiment Fourier-transform spectrometer, Appl. Opt., 44, 7218–7231, https://doi.org/10.1364/AO.44.007218, 2005.

Boone, C. D., Walker, K. A., and Bernath, P. F.: Version 3 retrievals for the atmospheric chemistry experiment Fourier transform spectrometer (ACE-FTS), The Atmospheric Chemistry Experiment ACE at 10: A Solar Occultation Anthology, A. Deepak Publishing, Hampton, Va., 2013.

Boone, C. D., Bernath, P. F., Cok, D., Jones, S. C., and Steffen, J.: Version 4 retrievals for the atmospheric chemistry experiment Fourier transform spectrometer (ACE-FTS) and imagers. Journal of Quantitative Spectroscopy and Radiative Transfer, 247, 106939, https://doi.org/10.1016/j.jqsrt.2020.106939, 2020.

Brewer, A. W.: Evidence for a world circulation provided by the measurements of helium and water vapour distribution in the stratosphere. Quarterly Journal of the Royal Meteorological Society, 75, 351–363, https://doi.org/10.1002/qj.49707532603, 1949.

Ceccherini, S., Carli, B., Raspollini, P., and Ridolfi, M.: Rigorous determination of stratospheric water vapor trends from MIPAS observations, Optics Express, 19(S3), A340-A360, https://doi.org/10.1364/OE.19.00A340, 2011.

Charlesworth, E., Plöger, F., Birner, T. et al. Stratospheric water vapor affecting atmospheric circulation. Nat Commun 14, 3925 (2023). https://doi.org/10.1038/s41467-023-39559-2

von Clarmann, T., Glatthor, N., Grabowski, U., Höpfner, M., Kellmann, S., Kiefer, M., Linden, A., Tsidu, G. M., Milz, M., Steck, T., Stiller, G. P., Wang, D. Y., Fischer, H., Funke, B., Gil-López, S., and López-Puertas, M.: Retrieval of temperature and

tangent altitude pointing from limb emission spectra recorded from space by the Michelson Interferometer for Passive Atmospheric Sounding (MIPAS). J. Geophys. Res. Atmos., 108(D23), 4719. https://doi.org/10.1029/2003jd003602, 2003.

von Clarmann, T., Höpfner, M., Kellmann, S., Linden, A., Chauhan, S., Funke, B., Grabowski, U., Glatthor, N., Kiefer, M., Schieferdecker, T., Stiller, G. P., and Versick, S.,: Retrieval of temperature, H2O, O3, HNO3, CH4, N2O, ClONO2 and ClO from MIPAS reduced resolution nominal mode limb emission measurements. Atmos. Meas. Tech., 2(1), 159-175. https://doi.org/10.5194/amt-2-159-2009, 2009.

Von Clarmann, T.: Validation of remotely sensed profiles of atmospheric state variables: strategies and terminology. Atmos. Chem. Phys., 6, 4311-4320, https://doi.org/10.5194/acp-6-4311-2006, 2006.

Dessler, A. E., Schoeberl, M. R., Wang, T., Davis, S. M., and Rosenlof, K. H.: Stratospheric water vapor feedback. Proc. Natl. Acad. Sci. U. S. A., 110, 18087–18091, https://doi.org/10.1073/pnas.1310344110, 2013.

Dinelli, B. M., Raspollini, P., Gai, M., Sgheri, L., Ridolfi, M., Ceccherini, S., Barbara, F., Zoppetti, N., Castelli, E., Papandrea, E., Pettinari, P., Dehn, A., Dudhia, A., Kiefer, M., Piro, A., Flaud, J.-M., López-Puertas, M., Moore, D., Remedios, J., and Bianchini, M.: The ESA MIPAS/Envisat level2-v8 dataset: 10 years of measurements retrieved with ORM v8.22, Atmos. Meas. Tech., 14, 7975–7998, https://doi.org/10.5194/amt-14-7975-2021, 2021.~~Dinelli, B. M., Raspollini, P., Gai, M., Sgheri, L., Ridolfi, M., Ceccherini, S., Barbara, F., Zoppetti, N., Castelli, E., Papandrea, E., Pettinari, P., Dehn, A., Dudhia, A., Kiefer, M., Piro, A., Flaud, J. M., López-Puertas, M., Moore, D., Remedios, J., and Bianchini, M.: The ESA MIPAS/ENVISAT Level2 v8 dataset: 10 years of measurements retrieved with ORM v8.22. Atmospheric Measurement Techniques Discussions, (March 2004), 1–36, https://doi.org/10.5194/amt-2021-215, 2021.~~

Fischer, H., Birk, M., Blom, C., Carli, B., Carlotti, M., von Clarmann, T., Delbouille, L., Dudhia, A., Ehhalt, D., Endemann, M., Flaud, J. M., Gessner, R., Kleinert, A., Koopman, R., Langen, J., López-Puertas, M., Mosner, P., Nett, H., Oelhaf, H., Perron, G., Remedios, J., Ridolfi, M., Stiller, G., and Zander, R.: MIPAS: An instrument for atmospheric and climate research. Atmospheric Chemistry and Physics, 8(8), 2151–2188, https://doi.org/10.5194/acp-8-2151-2008, 2008.

Flaud, J.-M., Piccolo, C., Carli, B., Perrin, A., Coudert, L.H., Teffo, J.-L., and Brown, L.R.: Molecular line parameters for the MIPAS (Michelson Interferometer for Passive Atmospheric Sounding) experiment, Atmos. Oceanic Opt., 16, 3, 172–182, March, 2003.

Froidevaux, L., Livesey, N.J., Read, W.G., Jiang, Y.B., Jimenez, C., Filipiak, M.J., Schwartz, M.J., Santee, M.L., Pumphrey, H.C., Jiang, J.H., Wu, D.L., Manney, G.L., Drouin, B.J., Waters, J.W., Fetzer, E.J., Bernath, P.F., Boone, C.D., Walker, K.A., Jucks,

K.W., Toon, G.C., Margitan, J.J., Sen, B., Webster, C.R., Christensen, L.E., Elkins, J.W., Atlas, E., Lueb, R.A., and Hendershot, R.: Early validation analyses of atmospheric profiles from EOS MLS on the Aura satellite. IEEE Transactions on Geoscience and Remote Sensing, 44(5), 1106–1121, https://doi.org/10.1109/TGRS.2006.864366, 2006.

Gettelman, A., Birner, T., Eyring, V., Akiyoshi, H., Bekki, S., Brühl, C., Dameris, M., Kinnison, D. E., Lefevre, F., Lott, F., Mancini, E., Pitari, G., Plummer, D. A., Rozanov, E., Shibata, K., Stenke, A., Struthers, H., and Tian, W.: The Tropical Tropopause Layer 1960–2100, Atmos. Chem. Phys., 9, 1621–1637, https://doi.org/10.5194/acp-9-1621-2009, 2009.

Gordon, I.E., Rothman, L.S., Hill, C., Kochanov, R.V., Tan, Y., Bernath, P.F., Birk, M., Boudon, V., Campargue, A., Chance, K.V., Drouin, B.J., Flaud, J.-M., Gamache, R.R., Hodges, J.T., Jacquemart, D., Perevalov, V.I., Perrin, A., Shine, K.P., Smith, M.-A.H., Tennyson, J., Toon, G.C., Tran, H., Tyuterev, V.G., Barbe, A., Császár, A.G., Devi, V.M., Furtenbacher, T., Harrison, J.J., Hartmann, J.-M., Jolly, A., Johnson, T.J., Karman, T., Kleiner, I., Kyuberis, A.A., Loos, J., Lyulin, O.M., Massie, S.T., Mikhailenko, S.N., Moazzen-Ahmadi, N., Müller, H.S.P., Naumenko, O.V., Nikitin, A.V., Polyansky, O.L., Rey, M., Rotger, M., Sharpe, S.W., Sung, K., Starikova, E., Tashkun, S.A., Vander Auwera, J., Wagner, G., Wilzewski, J., Wcisło, P., Yu, S., and Zak, E.J.: The HITRAN2016 molecular spectroscopic database. J. Quant. Spectrosc. Radiat. Transf., 203, 3-69. ISSN 0022-4073, https://doi.org/10.1016/j.jqsrt.2017.06.038, 2017.

Haenel, F. J., Stiller, G. P., von Clarmann, T., Funke, B., Eckert, E., Glatthor, N., Grabowski, U., Kellmann, S., Kiefer, M., Linden, A., and Reddmann, T.: Reassessment of MIPAS age of air trends and variability, Atmos. Chem. Phys., 15, 13161–13176, https://doi.org/10.5194/acp-15-13161-2015, 2015.

Hanisco, T.F., Moyer, E. J., Weinstock, E. M., St. Clair, J. M., Sayres, D. S., Smith, J. B., Lockwood, R., Anderson, J. G., Dessler, A. E., Keutsch, F. N., Spackman, J. R., Read, W. G., and Bui, T. P.: Geophys. Res. Lett., 34, L04814, doi:10.1029/2006GL027899, 2007.

Hegglin M.I., S. Tegtmeier, J. Anderson, L. Froidevaux, R. Fuller, B. Funke, A. Jones, G. Lingenfelser, J. Lumpe, D. Pendlebury, E. Remsberg, A. Rozanov, M. Toohey, J. Urban.: SPARC Data Initiative: Comparison of water vapor climatologies from international satellite limb sounders. J. Geophys. Res. Atmos., 118(20), 11,824-11,846, https://doi.org/10.1002/jgrd.50752, 2013.

Hegglin, M. I., Plummer, D. A., Shepherd, T. G., Scinocca, J. F., Anderson, J., Froidevaux, L., Funke, B., Hurst, D., Rozanov, A., Urban, J., von Clarmann, T., Walker, K. A., Wang, H. J., Tegtmeier, S., and Weigel, K.: Vertical structure of stratospheric water vapour trends derived from merged satellite data. Nat. Geosci., 7(10), 768–776, https://doi.org/10.1038/NGEO2236, 2014.

Högberg, C., Lossow, S., Khosrawi, F., Bauer, R., Walker, K. A., Eriksson, P., Murtagh, D. P., Stiller, G. P., Steinwagner, J., and Zhang, Q.: The SPARC water vapour assessment II: Profile-to-profile and climatological comparisons of stratospheric δd(H2O) observations from satellite. Atmos. Chem. Phys., 19(4), 2497–2526, https://doi.org/10.5194/acp-19-2497-2019, 2019.

Keller, W., and Borkowski, A.: Thin plate spline interpolation. J. Geod., 93, 1251–1269, https://doi.org/10.1007/s00190-019-01240-2, 2019.

Khosrawi, F., Lossow, S., Stiller, G. P., Rosenlof, K. H., Urban, J., Burrows, J. P., Damadeo, R. P., Eriksson, P., García-Comas, M., Gille, J. C., Kasai, Y., Kiefer, M., Nedoluha, G. E., Noël, S., Raspollini, P., Read, W. G., Rozanov, A., Sioris, C. E., Walker, K. A., and Weigel, K.: The SPARC water vapour assessment II: Comparison of stratospheric and lower mesospheric water vapour time series observed from satellites. Atmos. Meas. Tech., 11(7), 4435–4463. https://doi.org/10.5194/amt-11-4435-2018, 2018.

Kiefer, M., von Clarmann, T., Funke, B., García-Comas, M., Glatthor, N., Grabowski, U., Kellmann, S., Kleinert, A., Laeng, A., Linden, A., López-Puertas, M., Marsh, D. R., and Stiller, G. P.: IMK/IAA MIPAS temperature retrieval version 8: Nominal measurements. Atmos. Meas. Tech., 14(6), 4111–4138, https://doi.org/10.5194/amt-14-4111-2021, 2021.

Kiefer, M., Hurst, D. F., Stiller, G. P., Lossow, S., Vömel, H., Anderson, J., Azam, F., Bertaux, J.-L., Blanot, L., Bramstedt, K., Burrows, J. P., Damadeo, R., Dinelli, B. M., Eriksson, P., García-Comas, M., Gille, J. C., Hervig, M., Kasai, Y., Khosrawi, F., Murtagh, D., Nedoluha, G. E., Noël, S., Raspollini, P., Read, W. G., Rosenlof, K. H., Rozanov, A., Sioris, C. E., Sugita, T., von Clarmann, T., Walker, K. A., and Weigel, K.: The SPARC water vapour assessment II: biases and drifts of water vapour satellite data records with respect to frost point hygrometer records, Atmos. Meas. Tech., 16, 4589–4642, https://doi.org/10.5194/amt-16-4589-2023, 2023.

Kleinert, A., Aubertin, G., Perron, G., Birk, M., Wagner, G., Hase, F., Nett, H., and Poulin, R.: MIPAS Level 1B algorithms overview: Operational processing and characterization. Atmos. Chem. Phys., 7, 1395–1406, https://doi.org/10.5194/acp-7-1395-2007, 2007.

Kleinert, A., Birk, M., Perron, G., and Wagner, G.: Level 1b error budget for MIPAS on ENVISAT. Atmos. Meas. Tech., 11, 5657–5672, https://doi.org/10.5194/amt-11-5657-2018, 2018.

Konopka, P., Rolf, C., von Hobe, M., Khaykin, S. M., Clouser, B., Moyer, E., Ravegnani, F., D'Amato, F., Viciani, S., Spelten, N., Afchine, A., Krämer, M., Stroh, F., and Ploeger, F.: The dehydration carousel of stratospheric water vapor in the Asian summer monsoon anticyclone, Atmos. Chem. Phys., 23, 12935–12947, https://doi.org/10.5194/acp-23-12935-2023, 2023.

Kuang, Z., Toon, G. C., Wennberg, P. O., and Yung, Y. L.: Measured HDO/H2O ratios across the tropical tropopause. Geophys. Res. Lett., 30, 1–4, https://doi.org/10.1029/2003GL017023, 2003.

Lanzante, J. R.: Resistant, robust and non-parametric techniques for the analysis of climate data: Theory and examples, including applications to historical radiosonde station data. Int. J. Climatol., 16, 1197–1226. https://doi.org/10.1002/(SICI)1097-0088(199611)16:11<1197::AID-JOC89>3.0.CO;2-L, 1996.

LeTexier, H., Solomon, S., and Garcia, R.R.: The role of molecular hydrogen and methane oxidation in the water vapour budget of the stratosphere. Q. J. R. Meteorol. Soc., 114, 281–295, https://doi.org/10.1002/qj.49711448002, 1988.

Loew, A., Bell, W., Brocca, L., Bulgin, C. E., Burdanowitz, J., Calbet, X., Donner, R. V., Ghent, D., Gruber, A., Kaminski, T., Kerr, Y., Kunhikrishnan, P., Li, Z., Miralles, D., Mistelbauer, T., Nicolai-Shaw, N., Parinussa, R., Reimer, C., Rudiger, C., Schanze, J., Schrön, M., Smith, M., Su, Z., Trigo, I. F., van der Schalie, R., Wagner, W., and Zeng, Y.: Validation practices for satellite - based Earth observation data across communities. Rev. Geophys., 55(3), 779-817, https://doi.org/10.1002/2017RG000562, 2017.

Lossow, S., Steinwagner, J., Urban, J., Dupuy, E., Boone, C. D., Kellmann, S., Linden, A., Kiefer, M., Grabowski, U., Glatthor, N., Höpfner, M., Röckmann, T., Murtagh, D. P., Walker, K. A., Bernath, P. F., von Clarmann, T., and Stiller, G. P.: Comparison of HDO measurements from Envisat/MIPAS with observations by Odin/SMR and SCISAT/ACE-FTS. Atmos. Meas. Tech., 4, 1855–1874, https://doi.org/10.5194/amt-4-1855-2011, 2011.

Lossow, S., Khosrawi, F., Kiefer, M., Walker, K. A., Bertaux, J.-L., Blanot, L., Russell, J. M., Remsberg, E. E., Gille, J. C., Sugita, T., Sioris, C. E., Dinelli, B. M., Papandrea, E., Raspollini, P., García-Comas, M., Stiller, G. P., von Clarmann, T., Dudhia, A., Read, W. G., Nedoluha, G. E., Damadeo, R. P., Zawodny, J. M., Weigel, K., Rozanov, A., Azam, F., Bramstedt, K., Noël, S., Burrows, J. P., Sagawa, H., Kasai, Y., Urban, J., Eriksson, P., Murtagh, D. P., Hervig, M. E., Högberg, C., Hurst, D. F., and Rosenlof, K. H.: The SPARC water vapour assessment II: Profile-to-profile comparisons of stratospheric and lower mesospheric water vapour data sets obtained from satellites. Atmos. Meas. Tech., 12(5), 2693–2732. https://doi.org/10.5194/amt-12-2693-2019, 2019.

Lossow, S., Högberg, C., Khosrawi, F., Stiller, G. P., Bauer, R., Walker, K. A., Kellmann, S., Linden, A., Kiefer, M., Glatthor, N., von Clarmann, T., Murtagh, D. P., Steinwagner, J., Röckmann, T., and Eichinger, R.: A reassessment of the discrepancies in the annual variation of δD-H2O in the tropical lower stratosphere between the MIPAS and ACE-FTS satellite data sets. Atmos. Meas. Tech., 13(1), 287–308. https://doi.org/10.5194/amt-13-287-2020, 2020.

Merlivat, L., and Nief, G.: Fractionnement isotopique lors des changements d'état solide-vapeur et liquide-vapeur de l'eau à des températures inférieures à 0°C. Tellus A Dyn. Meteorol. Oceanogr., 19, 122, https://doi.org/10.3402/tellusa.v19i1.9756, 1967.

Milz, M., von Clarmann, T., Fischer, H., Glatthor, N., Grabowski, U., Höpfner, M., Kellmann, S., Kiefer, M., Linden, A., Mengistu Tsidu, G., Steck, T., Stiller, G. P., Funke, B., López-Puertas, M., and Koukouli, M. E.: Water vapor distributions measured with the Michelson Interferometer for Passive Atmospheric Sounding on board Envisat (MIPAS/Envisat). J. Geophys. Res. Atmos., 110(24), 1–14, https://doi.org/10.1029/2005JD005973, 2005.

Mote, P. W., Rosenlof, K. H., McIntyre, M. E., Carr, E. S., Gille, J. C., Holton, J. R., Kinnersley, J. S., Pumphrey, H. C., Russell, J. M., Waters, J. W.: An atmospheric tape recorder: The imprint of tropical tropopause temperatures on stratospheric water vapor. J. Geophys. Res. Atmos., 101, 3989–4006, https://doi.org/10.1029/95JD03422, 1996.

Moyer, E. J., Irion, F. W., Yung, Y. L., and Gunson, M. R.: ATMOS stratospheric deuterated water and implications for troposphere-stratosphere transport. Geophys. Res. Lett., 23, 2385–2388, https://doi.org/10.1029/96GL01489, 1996.

Murtagh, D., Frisk, U., Merino, F., Ridal, M., Jonsson, A., Stegman, J., Witt, G., Eriksson, P., Jiménez, C., Megie, G., de la Noë, J., Ricaud, P., Baron, P., Pardo, J. R., Hauchcorne, A., Llewellyn, E. J., Degenstein, D. A., Gattinger, R. L., Lloyd, N. D., Evans, W. F. J., McDade, I. C., Haley, C. S., Sioris, C., von Savigny, C., Solheim, B. H., McConnell, J. C., Strong, K., Richardson, E. H., Leppelmeier, G. W., Kyrölä, E., Auvinen, H., and Oikarinen, L.: An overview of the Odin atmospheric mission. Can. J. Phys., 80, 309–319, https://doi.org/10.1139/p01-157, 2002.

Nassar, R., Bernath, P. F., Boone, C. D., Manney, G. L., Mcleod, S. D., Rinsland, C. P., Skelton, R., and Walker, K. A.: Stratospheric abundances of water and methane based on ACE-FTS measurements. Geophys. Res. Lett., 32, 2–6, https://doi.org/10.1029/2005GL022383, 2005.

Nedoluha, G. E., Kiefer, M., Lossow, S., Gomez, R. M., Kämpfer, N., Lainer, M., Forkman, P., Christensen, O. M., Oh, J. J., Hartogh, P., Anderson, J., Bramstedt, K., Dinelli, B. M., Garcia-Comas, M., Hervig, M., Murtagh, D., Raspollini, P., Read, W. G., Rosenlof, K., Stiller, G. P., and Walker, K. A.: The SPARC water vapor assessment II: Intercomparison of satellite and

ground-based microwave measurements. Atmos. Chem. Phys., 17(23), 14543–14558, https://doi.org/10.5194/acp-17-14543-2017, 2017.

Payne, V. H., Noone, D., Dudhia, A., Piccolo, C., and Grainger, R. G.: Global satellite measurements of HDO and implications for understanding the transport of water vapor into the stratosphere. Q. J. R. Meteorol. Soc., 133, 1459–1471, https://doi.org/10.1002/qj.127, 2007.

Plaza, N. P., Podglajen, A., Peña-Ortiz, C., and Ploeger, F.: Processes influencing lower stratospheric water vapor in monsoon anticyclones: Insights from Lagrangian modeling. Atmos. Chem. Phys., 21(12), https://doi.org/10.5194/acp-21-9585-2021, 2021.

Randel, W. J., Moyer, E., Park, M., Jensen, E., Bernath, P., Walker, K., and Boone, C.: Global variations of HDO and HDO/H2O ratios in the upper troposphere and lower stratosphere derived from ACE-FTS satellite measurements. J. Geophys. Res. Atmos., 117, 1–16, https://doi.org/10.1029/2011JD016632, 2012.

Raspollini, P., A. Piro, D. Hubert, A. Keppens, J.-C. Lambert, G. Wetzel, D. Moore, S. Ceccherini, M. Gai, F. Barbara, N. Zoppetti, with MIPAS Quality Working Group, MIPAS validation teams, MIPAS IDEAS+ (Instrument Data quality Evaluation and Analysis Service) team. ENVIromental SATellite (ENVISAT) MICHELSON INTERFEROMETER for PASSIVE ATMOSPHERIC SOUNDING (MIPAS). ESA Level 2 version 8.22 products - Product Quality Readme File. ESA-EOPG-EBA-TN-5, issue 1.0, 2020.

Raspollini, P., Arnone, E., Barbara, F., Bianchini, M., Carli, B., Ceccherini, S., Chipperfield, M. P., Dehn, A., Della Fera, S., Dinelli, B. M., Dudhia, A., Flaud, J.-M., Gai, M., Kiefer, M., López-Puertas, M., Moore, D. P., Piro, A., Remedios, J. J., Ridolfi, M., Sembhi, H., Sgheri, L., and Zoppetti, N.: Level 2 processor and auxiliary data for ESA Version 8 final full mission analysis of MIPAS measurements on ENVISAT, Atmos. Meas. Tech., 15, 1871–1901, https://doi.org/10.5194/amt-15-1871-2022, 2022

Read, W. G., Stiller, G., Lossow, S., Kiefer, M., Khosrawi, F., Hurst, D., Vömel, H., Rosenlof, K., Dinelli, B. M., Raspollini, P., Nedoluha, G. E., Gille, J. C., Kasai, Y., Eriksson, P., Sioris, C. E., Walker, K. A., Weigel, K., Burrows, J. P., and Rozanov, A.: The SPARC Water Vapor Assessment II: assessment of satellite measurements of upper tropospheric humidity. Atmos. Meas. Tech., 15(11), 3377–3401, https://doi.org/10.5194/amt-15-3377-2022, 2022.

Ridolfi, M., Carli, B., Carlotti, M., von Clarmann, T., Dinelli, B. M., Dudhia, A., Flaud, J.-M., Höpfner, M., Morris, P. E., Raspollini, P., Stiller, G., and Wells, R. J.: Optimized forward model and retrieval scheme for MIPAS near-real-time data processing, Appl. Opt., 39(9), 1323–1340, https://doi.org/10.1364/AO.39.001323, 2000.

Riese, M., Ploeger, F., Rap, A., Vogel, B., Konopka, P., Dameris, M., and Forster, P.: Impact of uncertainties in atmospheric mixing on simulated UTLS composition and related radiative effects, J. Geophys. Res. Atmos., 117, 1–10, https://doi.org/10.1029/2012JD017751, 2012.

Rothman L.S., C. P. Rinsland, A. Goldman et al., "The HITRAN Molecular Spectroscopic Database and HAWKS (HITRAN Atmospheric Workstation): 1996 Edition", *Journal Of Quantitative Spectroscopy and Radiative Transfer* **60**, 665-710 (1998).

Rosenlof, K. H., Oltmans, S. J., Kley, D., Russell III, J. M., Chiou, E.-W., Chu, W. P., Johnson, D. G., Kelly, K. K., Michelsen, H. A., Nedoluha, G. E., Remsberg, E. E., Toon, G. C., and McCormick, M. P.: Stratospheric water vapor increases over the past half-century, Geophys. Res. Lett., 28(7), 1195–1198, https://doi.org/10.1029/2000GL012502, 2001.

Scheepmaker, R. A., aan de Brugh, J., Hu, H., Borsdorff, T., Frankenberg, C., Risi, C., Hasekamp, O., Aben, I., and Landgraf, J.: HDO and H2O total column retrievals from TROPOMI shortwave infrared measurements, Atmos. Meas. Tech., 9(8), 3921–3937, https://doi.org/10.5194/amt-9-3921-2016, 2016.

Schneider, A., Borsdorff, T., aan de Brugh, J., Aemisegger, F., Feist, D. G., Kivi, R., Hase, F., Schneider, M., and Landgraf, J.: First data set of H2O/HDO columns from the Tropospheric Monitoring Instrument (TROPOMI), Atmos. Meas. Tech., 13(1), 85–100, https://doi.org/10.5194/amt-13-85-2020, 2020.

Sheese, P. E., Boone, C. D., and Walker, K. A.: Detecting physically unrealistic outliers in ACE-FTS atmospheric measurements, Atmos. Meas. Tech., 8, 741–750, https://doi.org/10.5194/amt-8-741-2015, 2015.

Sheese, P. E., Walker, K. A., Boone, C. D., McLinden, C. A., Bernath, P. F., Bourassa, A. E., Burrows, J. P., Degenstein, D. A., Funke, B., Fussen, D., Manney, G. L., McElroy, C. T., Murtagh, D., Randall, C. E., Raspollini, P., Rozanov, A., Russell III, J. M., Suzuki, M., Shiotani, M., Urban, J., von Clarmann, T., and Zawodny, J. M.: Validation of ACE-FTS version 3.5 NOy species profiles using correlative satellite measurements, Atmos. Meas. Tech., 9(12), 5781–5810, https://doi.org/10.5194/amt-9-5781-2016, 2016.

Sheese, P. E., Walker, K. A., Boone, C. D., Bernath, P. F., Froidevaux, L., Funke, B., Raspollini, P., and von Clarmann, T.: ACE-FTS ozone, water vapour, nitrous oxide, nitric acid, and carbon monoxide profile comparisons with MIPAS and MLS, J. Quant. Spectrosc. Radiat. Transf., 186, 63–80, https://doi.org/10.1016/j.jqsrt.2016.06.026, 2017.

Solomon, S., Qin, D., Manning, M., Chen, Z., Marquis, K. B., Averyt, M. Tignor, M., and Miller, H. L.: Fourth assessment report of the Intergovernmental Panel on Climate Change: Important observations and conclusions, Curr. Sci., 92, 1034, 2007.

Solomon, S., Rosenlof, K. H., Portmann, R. W., Daniel, J. S., Davis, S. M., Sanford, T. J., and Plattner, G. K.: Contributions of stratospheric water vapor to decadal changes in the rate of global warming, Science, 327, 1219–1223, 10.1126/science.1182488, 2010.

Speidel, J., Stiller, G., Glatthor, N., Kiefer, M., Lossow, S., and von Clarmann, T.: Seasonal variations of stratospheric deuterated water in the Asian summer monsoon, Geophysical Research Abstracts, Vol. 20. EGU General Assembly 2018, EGU2018-14341, 2018.

Steinwagner, J., Milz, M., Von Clarmann, T., Glatthor, N., Grabowski, U., Höpfner, M., Stiller, G. P., and Röckmann, T.: HDO measurements with MIPAS, Atmos. Chem. Phys., 7, 2601–2615, https://doi.org/10.5194/acp-7-2601-2007, 2007.

Steinwagner, J., Fueglistaler, S., Stiller, G., Von Clarmann, T., Kiefer, M., Borsboom, P. P., Van Delden, A., and Röckmann, T.: Tropical dehydration processes constrained by the seasonality of stratospheric deuterated water, Nat. Geosci., 3, 262–266, https://doi.org/10.1038/ngeo822, 2010.

Stiller, G. P., von Clarmann, T., Haenel, F., Funke, B., Glatthor, N., Grabowski, U., Kellmann, S., Kiefer, M., Linden, A., Lossow, S., and López-Puertas, M.: Observed temporal evolution of global mean age of stratospheric air for the 2002 to 2010 period, Atmos. Chem. Phys., 12, 3311–3331, https://doi.org/10.5194/acp-12-3311-2012, 2012.

~~Raspollini, P., A. Piro, D. Hubert, A. Keppens, J.-C. Lambert, G. Wetzel, D. Moore, S. Ceccherini, M. Gai, F. Barbara, N. Zoppetti, with MIPAS Quality Working Group, MIPAS validation teams, MIPAS IDEAS+ (Instrument Data quality Evaluation and Analysis Service) team. ENVIromental SATellite (ENVISAT) MICHELSON INTERFEROMETER for PASSIVE ATMOSPHERIC SOUNDING (MIPAS). ESA Level 2 version 8.22 products – Product Quality Readme File. ESA-EOPG-EBA-TN-5, issue 1.0, 2020.~~

Toohey, M., and Strong, K.: Estimating biases and error variances through the comparison of coincident satellite measurements, J. Geophys. Res. Atmos., 112, 1–12, https://doi.org/10.1029/2006JD008192, 2007.

Tuinenburg, O. A., Risi, C., Lacour, J. L., Schneider, M., Wiegele, A., Worden, J., Kurita, N., Duvel, J. P., Deutscher, N., Bony, S., Coheur, P. F., and Clerbaux, C.: Moist processes during MJO events as diagnosed from water isotopic measurements from the IASI satellite, J. Geophys. Res., 120(20), 10,619-10,636, https://doi.org/10.1002/2015JD023461, 2015.

Vogel, B., Feck, T., and Groobß, J. U.: Impact of stratospheric water vapor enhancements caused by CH4 and H2O increase on polar ozone loss, J. Geophys. Res. Atmos., 116, 1–11, https://doi.org/10.1029/2010JD014234, 2011.

Walker, K. A., Sheese, P. E., and Zou, J.: Validation Studies for the Atmospheric Chemistry Experiment Fourier Transform Spectrometer (ACE-FTS), OSA Optical Sensors and Sensing Congress 2021 (AIS, FTS, HISE, SENSORS, ES), Optica Publishing Group, FTh4G.4, 2021.

Wang, T., Zhang, Q., Lossow, S., Chafik, L., Risi, C., Murtagh, D., and Hannachi, A.: Stable Water Isotopologues in the stratosphere retrieved from Odin/SMR measurements, Remote Sens., 10, https://doi.org/10.3390/rs10020166, 2018.

Wang, X., Dessler, A. E., Schoeberl, M. R., Yu, W., and Wang, T.: Impact of convectively lofted ice on the seasonal cycle of water vapor in the tropical tropopause layer, Atmos. Chem. Phys., 19, https://doi.org/10.5194/acp-19-14621-2019, 2019.

Waters, J. W., Froidevaux, L., Harwood, R. S., Jarnot, R. F., Pickett, H. M., Read, W. G., Siegel, P. H., Cofield, R. E., Filipiak, M. J., Flower, D. A., Holden, J. R., Lau, G. K., Livesey, N. J., Manney, G. L., Pumphrey, H. C., Santee, M. L., Wu, D. L., Cuddy, D. T., Lay, R. R., Loo, M. S., Perun, V. S., Schwartz, M. J., Stek, P. C., Thurstans, R. P., Boyles, M. A., Chandra, K. M., Chavez, M. C., Gun-Shing Chen, Chudasama, B. V., Dodge, R., Fuller, R. A., Girard, M. A., Jiang, J. H., Yibo Jiang, Knosp, B. W., LaBelle, R. C., Lam, J. C., Lee, K. A., Miller, D., Oswald, J. E., Patel, N. C., Pukala, D. M., Quintero, O., Scaff, D. M., Van Snyder, W., Tope, M. C., Wagner, P. A., and Walch, M. J.: The Earth Observing System Microwave Limb Sounder (EOS MLS) on the aura satellite, IEEE Trans. Geosci. Remote Sens., 44(5), 1075–1092, https://doi.org/10.1109/TGRS.2006.873771, 2006.

Wetzel, G., Oelhaf, H., Berthet, G., Bracher, A., Cornacchia, C., Feist, D. G., Fischer, H., Fix, A., Iarlori, M., Kleinert, A., Lengel, A., Milz, M., Mona, L., Müller, S. C., Ovarlez, J., Pappalardo, G., Piccolo, C., Raspollini, P., Renard, J.-B., Rizi, V., Rohs, S., Schiller, C., Stiller, G., Weber, M., and Zhang, G.: Validation of MIPAS-ENVISAT H2O operational data collected between July 2002 and March 2004, Atmos. Chem. Phys., 13(11), 5791-5811, https://doi.org/10.5194/acp-13-5791-2013, 2013.